Efficient Training of Minimal and Maximal Low-Rank Recurrent Neural Networks

Anushri Arora
Department of Computer Science
Princeton University
aa1698@princeton.edu

Jonathan W. Pillow
Princeton Neuroscience Institute
Princeton University
pillow@princeton.edu

Abstract

Low-rank recurrent neural networks (RNNs) provide a powerful framework for characterizing how neural systems solve complex cognitive tasks. However, fitting and interpreting these networks remains an important open problem. In this paper, we develop new methods for efficiently fitting low-rank RNNs in “teacher-training” settings. In particular, we build upon the neural engineering framework (NEF), in which RNNs are viewed as approximating an ordinary differential equation (ODE) of interest using a set of random nonlinear basis functions. This view provides geometric insight into how the choice of neural nonlinearity (e.g. tanh, ReLU) and the distribution of model parameters affects an RNN’s representational capacity. We show that this perspective leads to an online training method that achieves higher accuracy with smaller networks than previous methods such as FORCE, and outperform backprop-trained networks of similar size while requiring substantially less training time. We then consider the problem of finding minimal and maximal low-RNNs for approximating a target dynamical system. We show that a variant of orthogonal matching pursuit (OMP) can be used to find the smallest RNN for a dynamical system of interest. At the other extreme, a dual space formulation allows for efficient fitting of infinite low-rank RNNs, which provide a Gaussian Process (GP) prior over dynamical systems. We use the resulting GP marginal likelihood to optimize the hyperparameters governing neural activation functions, which leads to improved training performance even for finite RNNs. Finally, we describe active learning methods for low-rank RNNs, which speed up training through the selection of maximally informative activity patterns.

1 Introduction

Recurrent neural networks (RNNs) are a popular tool for characterizing the computational properties of neural populations and the dynamics underlying complex cognitive tasks [1–6]. Previous work has proposed a variety of methods for training RNNs to implement a dynamical system or generate a target signal of interest, including reservoir computing [7, 8], FORCE [9, 10], and back-propagation [11–13]. However, trained RNNs remain difficult to interpret. Common approaches tend to use search methods to identify fixed points or “slow points”, and then use dimensionality-reduction methods to visualize projected flow fields around these points [12, 14]. However, fixed-point finding algorithms are difficult to apply to high-dimensional systems, and it is often unclear how accurately low-D projections reflect a network’s true dynamics [2, 15].

To overcome these difficulties, recent work has focused on “low-rank RNNs”, in which the recurrent weight matrix is constrained to have low rank [3, 16, 6, 17]. This literature has shown that a wide variety of tasks can be implemented in low-rank RNNs, which exhibit dynamics whose dimension is limited by the rank of the recurrent weight matrix and number of input dimensions.

39th Conference on Neural Information Processing Systems (NeurIPS 2025).

A parallel arm of research has focused on methods for embedding low-dimensional quantities into high-dimensional network activity [18–23]. Of particular relevance to our work is the Neural Engineering Framework (NEF) which provides an analytical method for determining connection weights between neurons that implement a desired function or dynamical system. This is achieved via distributed representations, where each neuron characterizes the target function through a random nonlinear projection, forming diverse tuning curves across the population. Network connection weights are then obtained by finding the optimal linear combination of these nonlinear projections via least-squares regression, enabling complex function approximation.
This approach is closely related to sparse linear approximation methods that seek to use an overcomplete library of basis functions to fit the ODEs [24, 25]. For instance, SINDY proposes using sparse regression over a pre-specified polynomial basis to reconstruct a system's dynamics [26]. Moving-window approaches [27] employ a sliding-horizon scheme: solving a constrained optimization at each time window, and using statistical tests to prune irrelevant basis functions, thereby maintaining parsimony over time. More recently, [28] considered linear splines as basis functions, preserving network expressivity while yielding analytically tractable update rules that improve interpretability. However, these methods rely on explicit parametric representations of the system dynamics. In contrast, neural-network Gaussian processes (NNGPs) offer a nonparametric alternative, encoding priors over function classes defined by infinite-width neural networks [29–31]. While this has traditionally been limited to feedforward networks, recent work has extended it to recurrent settings via untied-weight constructions [32–34].

Here we present a unified framework for designing and training low-rank RNNs that implement a target dynamical system of interest. We begin with an offline method based on NEF, where each neuron acts as a nonlinear basis function and least-squares regression embeds a known ODE into the network. This yields a geometric view of universal approximation, illustrating how nonlinearity choices ($tanh$ vs ReLU) shape representational capacity. We then extend this to an online setting using a recursive least-squares update, and show that our method outperforms FORCE and BP in network accuracy and convergence speed. Next, we address the critical question of basis selection: using a variant of orthogonal matching pursuit (OMP), we identify the minimal set of basis functions needed to implement a given dynamics. We then consider infinite low-rank RNNs, which converge to a Gaussian process (GP), enabling principled initialization by maximizing the marginal likelihood over hyperparameters governing neural activation functions. Finally, we introduce an active learning strategy to efficiently select informative datapoints, further reducing training time and data requirements [1].

2 Background: low-rank recurrent neural networks

Consider a population of d rate-based neurons with membrane potentials $\mathbf{x} = [x_1, \dots, x_d]^\top$ and firing rates $\phi(\mathbf{x}) = [\phi(x_1), \dots, \phi(x_d)]^\top$, where $\phi(\cdot)$ is a scalar nonlinearity mapping the membrane potential to firing rate (e.g., sigmoid, tanh, ReLU). The dynamics of a generic RNN are given by a vector ordinary differential equation and a linear output:

$$\dot{\mathbf{x}} = -\mathbf{x} + J\phi(\mathbf{x}) + B\mathbf{u}, \quad \mathbf{z} = W\phi(\mathbf{x}) \tag{1}$$

where $J \in \mathbb{R}^{d\times d}$ is the recurrent weight matrix, $B \in \mathbb{R}^{d\times d_{in}}$ the input matrix, $\mathbf{u}$ is a d_{in}-dimensional input signal, and $W \in \mathbb{R}^{d_{out}\times d}$ a readout matrix. This network becomes a *low-rank RNN* if the recurrent weight matrix J has reduced rank $r < d$, thus factorizing as:

$$J = MN^\top = \sum_{i=1}^{r} \mathbf{m}_i \mathbf{n}_i^\top, \quad \text{where } \{M, N \in \mathbb{R}^{d\times r}\} \tag{2}$$

Here $\mathbf{m}_i, \mathbf{n}_i$ are columns of M, N respectively. In this case, the network state $x(t)$ evolves within a subspace of at most $r + d_{in}$ dimensions [3, 6], with activity in the remaining dimensions decaying due to the term $(-\mathbf{x})$. Thus, the network state vector can be expressed as:

$$\mathbf{x}(t) = M\boldsymbol{\kappa}(t) + B\mathbf{v}(t), \tag{3}$$

where $\boldsymbol{\kappa}(t)$ represents latent recurrent activity and $\mathbf{v}(t)$ denotes low-pass filtered inputs [6, 17]. Finally, $\dot{\boldsymbol{\kappa}} = F(\boldsymbol{\kappa}, \mathbf{u})$ represents the differential equation that governs the low-dimensional recurrent dynamics, where F is a nonlinear function of the latent state $\boldsymbol{\kappa}$ and input $\mathbf{u}$.

[1]Code: https://github.com/anushri10/Efficient-Training-of-Minimal-and-Maximal-Low-Rank-RNNs.git

3 An alternate view of low-rank RNNs

Standard approaches to training low-rank RNNs involves optimizing the parameters $\{N, M, B, W\}$ via back-propagation [17]. Here we consider an alternative approach, which amounts to solving a least squares regression problem with a set of random nonlinear basis functions.

We begin by considering the problem of embedding an arbitrary low-dimensional dynamical system into a low-rank RNN. Specifically, we wish to set the model parameters so that $\mathbf{z}$ obeys the dynamics of an particular "target" ODE:

$$\dot{\mathbf{z}} = g(\mathbf{z}) \tag{4}$$

for some function g. We will then identify this output with the latent vector defining the network's activity in the recurrent subspace: $\mathbf{z}(t) \triangleq \boldsymbol{\kappa}(t)$. This implies that the dimensionality of the output is equal to the rank of the network, $r = d_{out}$, and constrains the output weights to be the projection operator onto the column space of M, that is, $W = M(M^\top M)^{-1}$. (If the target output is lower dimensional than the rank of the network r, we can truncate $\mathbf{z}$ to take only its first d_{out} elements).

We are then left with the problem of setting the network weights M, N, and input weights B so that the latent vector $\mathbf{z}(t)$ evolves according to (eq. 4). For simplicity, consider the rank-1 case where $\mathbf{z}$ is scalar. This corresponds to an RNN weight matrix $J = \mathbf{m}\mathbf{n}^\top$. Assume that the input is also scalar, and that the input vector $\mathbf{b} \in \mathbb{R}^d$ is orthogonal to $\mathbf{m}$ (although we relax this constraint in SI C). The network state can then be decomposed as a time-varying linear combination of $\mathbf{m}$ and $\mathbf{b}$ [16, 6, 17] (eq. 3):

$$\mathbf{x}(t) = \mathbf{m}\mathbf{z}(t) + \mathbf{b}\mathbf{v}(t), \tag{5}$$

where $\mathbf{v}(t)$ represents the low-pass filtered input, resulting from the linear dynamical system $\dot{\mathbf{v}} = -\mathbf{v} + \mathbf{u}(t)$. The fact that $\mathbf{m}$ and $\mathbf{b}$ are orthogonal means that we can write the dynamics that govern the latent variable explicitly as:

$$\dot{\mathbf{z}} = -\mathbf{z} + \mathbf{n}^\top \phi(\mathbf{m}\mathbf{z} + \mathbf{b}\mathbf{v}) \tag{6}$$

a result shown previously in [17], and which is schematized in Fig. 1. Our goal of embedding an arbitrary ODE $g(\mathbf{z})$ into the network can be now viewed as setting the model parameters so that

$$g(\mathbf{z}) + \mathbf{z} \;\approx\; \mathbf{n}^\top \phi(\mathbf{m}\mathbf{z} + \mathbf{b}\mathbf{v}) \tag{7}$$

To achieve this, note that the right-hand-side can be viewed as a linear combination of terms $\phi(m_i\mathbf{z} + b_i\mathbf{v})$ with weights n_i, for $i \in \{1, \ldots, d\}$. Each of these terms can be viewed as a nonlinear basis function in $\mathbf{z}$. If ϕ is the hyperbolic tangent function, each such term is a shifted, scaled $\tanh$ function in $\mathbf{z}$, where m_i is the slope and $b_i v$ is the offset. This means that we can view the problem of embedding $g(\mathbf{z})$ into a low-rank RNN as the problem of setting $\mathbf{m}$ and $\mathbf{b}$ to build an appropriate set of basis functions, and setting $\mathbf{n}$ so that the linear combination of basis functions approximates $g(\mathbf{z}) + \mathbf{z}$. This approach formalizes the connection between low-rank RNNs and the NEF [18, 21], and shows that a low-rank RNN corresponds to a neural ODE with a single hidden layer [35–37].

Already, this perspective makes an important limitation clear: if the inputs $\mathbf{v}(t)$ are zero, the basis functions are all odd-symmetric (that is, $g(m_i\mathbf{z}) = -g(-m_i\mathbf{z})$ for all $\mathbf{z}$), crossing the origin only at zero. (see Fig. 1C). Because $-\mathbf{z}$ is also odd-symmetric, and the linear combination of odd-symmetric functions is odd-symmetric, this means that in the absence of inputs, the network can only capture the odd-symmetric component of $g(\mathbf{z})$. A low-rank RNN is therefore not a universal approximator unless it has inputs, or equivalently, different biases or offsets to each neuron (similar to general RNNs). If the ϕ is instead taken to be ReLU, the problem is even more severe: each basis function is a linear function with non-zero slope on either $\mathbf{z} > 0$ or $\mathbf{z} < 0$. Thus the network can only approximate $g(\mathbf{z})$ that are piecewise linear functions broken at the origin. (SI Fig. 7).

If we set the filtered input to be the constant $\mathbf{v} = 1$, we see that the problem of embedding an arbitrary ODE in a low-rank RNN amounts to fitting the ODE in a basis of shifted and scaled basis functions in $\mathbf{z}$. To achieve this, we propose to sample the scales (elements of $\mathbf{m}$) and offsets (elements of $\mathbf{b}$) to obtain a random basis, and then fit $\mathbf{n}$ by least-squares regression, namely:

$$\hat{\mathbf{n}} = (\phi(\mathbf{z}_{grid}\mathbf{m}^\top + \mathbf{b}^\top)^\top \phi(\mathbf{z}_{grid}\mathbf{m}^\top + \mathbf{b}^\top))^{-1} \phi(\mathbf{z}_{grid}\mathbf{m}^\top + \mathbf{b}^\top)^\top \big(g(\mathbf{z}_{grid}) + \mathbf{z}_{grid}\big) \tag{8}$$

where $\mathbf{z}_{grid}$ denotes a grid of points at which we wish to fit $g(\mathbf{z})$. Note that we could use weighted least squares if we care more about accurately approximating certain regions of $g(\mathbf{z})$, or add a small

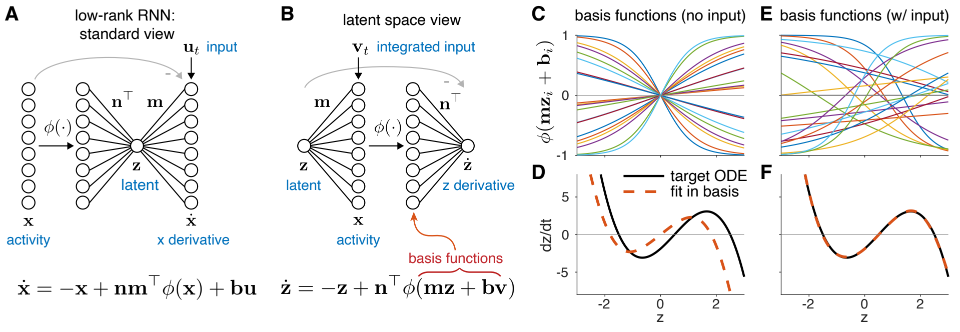
A
low-rank RNN: standard view
$\mathbf{u}_t$ input
$\phi(\cdot)$
$\mathbf{n}^\top$
$\mathbf{m}$
$\mathbf{z}$
latent
$\mathbf{x}$
activity
$\dot{\mathbf{x}}$
x derivative
$\dot{\mathbf{x}} = -\mathbf{x} + \mathbf{n}\mathbf{m}^\top\phi(\mathbf{x}) + \mathbf{b}\mathbf{u}$
B
latent space view
$\mathbf{v}_t$ integrated input
$\mathbf{m}$
$\phi(\cdot)$
$\mathbf{n}^\top$
$\mathbf{z}$
latent
$\mathbf{x}$
activity
$\dot{\mathbf{z}}$
z derivative
basis functions
$\dot{\mathbf{z}} = -\mathbf{z} + \mathbf{n}^\top\phi(\mathbf{m}\mathbf{z} + \mathbf{b}\mathbf{v})$
C
basis functions (no input)
$\phi(\mathbf{m}z_i + \mathbf{b}_i)$
E
basis functions (w/ input)
D
target ODE
fit in basis
dz/dt
z
F
z

Figure 1: Two equivalent views of low-rank RNNs. **(A)** Standard view of rank-1 RNN with 8 neurons $\mathbf{x}$ and 1 latent dimension $\mathbf{z}$. **(B)** Alternate view of the same network, now framed in terms of the dynamics of latent $\mathbf{z}$. This shows that a low-rank RNN is equivalent to a neural ODE with a single hidden layer [35]. **(C)** Basis functions obtained by sampling slope parameters $m_i \sim \mathcal{N}(0,1)$, but without input ($\mathbf{v}_t = 0$). **(D)** Attempting to fit an example ODE using this basis recovers only the odd-symmetric component, since all basis functions are odd symmetric. **(E)** Adding inputs allows basis functions have random horizontal offsets. Here we sampled the input weights $\mathbf{b}_i \sim \mathcal{N}(0,1)$ and set input $\mathbf{v}_t = 1$. (Note that this could also be obtained by using per-neuron "biases"). **(F)** Least squares fitting of $\mathbf{n}$ using the basis from (E) provides good fit to the target ODE.

ridge penalty if the design matrix (whose columns are given by the basis functions evaluated at $\mathbf{z}_{grid}$) is ill-conditioned.

Fig. 1 shows an illustration of this approach for an example ODE, here chosen to be a cubic polynomial with two stable fixed points and one unstable fixed point. Note that the network cannot approximate $g(\mathbf{z})$ when the inputs are set to zero (Fig. 1C-D), but can do so with near-perfect accuracy when both the $\mathbf{m}$ vector and the (constant) inputs $\mathbf{b}$ are drawn from a Gaussian distribution (Fig. 1E-F).

3.1 Multi-dimensional dynamical systems

We can apply this same regression-based approach to higher-dimensional nonlinear dynamical systems, where rank $r = \dim(\mathbf{z}) > 1$. In two dimensions, the basis functions are given by $\phi(m_{1i}z_1 + m_{2i}z_2 + b_i)$, which are scaled, shifted $\tanh$ functions with a random orientation (Fig. 2A). Approximating a 2D dynamical system with a rank-2 RNN can then be written as the problem of fitting two different nonlinear functions $g_1(\mathbf{z})$ and $g_2(\mathbf{z})$ using two different linear combinations of the same 2D basis functions:

$$g(\mathbf{z}) = \begin{bmatrix} g_1(\mathbf{z}) \\ g_2(\mathbf{z}) \end{bmatrix} \approx -\begin{bmatrix} z_1 \\ z_2 \end{bmatrix} + \begin{bmatrix} \mathbf{n}_1^\top \phi(M\mathbf{z} + \mathbf{b}) \\ \mathbf{n}_2^\top \phi(M\mathbf{z} + \mathbf{b}) \end{bmatrix}, \tag{9}$$

where $M = [\mathbf{m}_1 \mathbf{m}_2]$ is a $d \times 2$ matrix whose columns define the slope and orientation of each basis function, $\mathbf{b}$ is once again a column vector of offsets, and we have assumed constant input ($\mathbf{v} = 1$). Note once again that if we do not include inputs, the basis functions are all radially odd-symmetric around the origin. Thus, once again, the RNN will only be able to capture radially odd-symmetric $g(\mathbf{z})$, and is not a universal approximator unless we include nonzero offsets $\mathbf{b}\mathbf{v} \neq 0$.

To embed a given multi-dimensional ODE $g(\mathbf{z})$ into a low-rank RNN, we once again generate a random basis by sampling the elements of $M \in \mathbb{R}^{d\times 2}$ and $\mathbf{b} \in \mathbb{R}^d$ from a Gaussian distribution. The problem factorizes into learning each column vector $\mathbf{n}_i$ for each dimension of the g, we have:

$$\hat{\mathbf{n}}_i = (\phi(Z_{grid}M^\top + \mathbf{b}^\top)^\top \phi(Z_{grid}M^\top + \mathbf{b}^\top))^{-1}\phi(Z_{grid}M^\top + \mathbf{b}^\top)^\top \big(g(Z_{grid}) + Z_{grid}\big), \tag{10}$$

for $i = 1, 2$. This differs from the 1D case above only in that Z_{grid} is now a r-column matrix of grid points, where each row contains the coordinates of a single point in $\mathbf{z}$. Note that these grid points need not be uniformly sampled; we could sample them from an arbitrary distribution, or use a collection of points from simulating the ODE from a variety of starting points (SI E.2).
Fig. 2 shows an application to an example 2-dimensional nonlinear ODE, in this case containing a stable limit cycle. Note that this 2D system is highly nonlinear and not radially odd-symmetric, so once again, embedding the system in a low-rank RNN fails if we do not include inputs (or per-neuron biases, SI A.2).

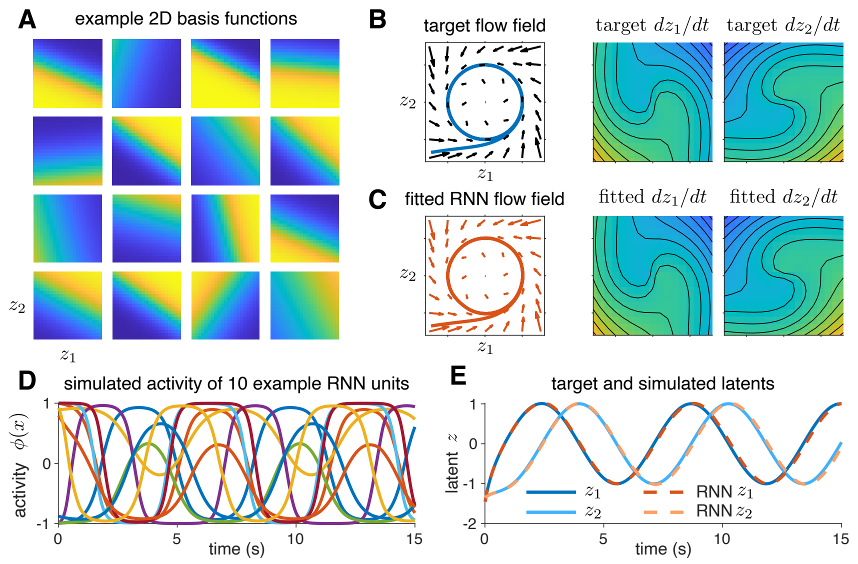

Figure 2: Embedding a 2-dimensional nonlinear ODE into a rank-2 RNN. **(A)** Example basis functions obtained by sampling M and $\mathbf{b}$ coefficients from a zero-mean Gaussian, producing randomly oriented, scaled, and shifted hyperbolic tangent functions. **(B)** A target two-dimensional nonlinear dynamical system, containing a stable limit cycle on a circle of radius one, represented as a flow field (left), or by its component functions $g_1(\mathbf{z}) = \frac{dz_1}{dt}$ and $g_2(\mathbf{z}) = \frac{dz_2}{dt}$ (right). **(C)** Least squares fitting of weight vectors $\mathbf{n}_1$ and $\mathbf{n}_2$ produces a near perfect match to the target flow field, and functions g_1 and g_2. **(D)** Output firing rates $\phi(x_i)$ for 10 example units (i.e $i \in \{1, \ldots, 10\}$) during the red example trajectory shown in panel C. **(E)** Simulated trajectories from the true ODE (blue trace in panel B) and latent variable of the fitted RNN (red trace from panel C), plotted as a function of time, showing good agreement between the target ODE and the RNN output. Note that fitting was closed-form, and did not require backprop-through-time.

4 Comparison with backpropagation (BP) and FORCE

Recursive least squares for online fitting: The previous sections present an offline learning approach for $\mathbf{n}$ via a basis design matrix composed of all points on the grid ($\mathbf{z}$) at which the target ODE ($g(\mathbf{z})$) is evaluated. Here, we adapt this framework to online learning—a format used by most state-of-the-art RNN training algorithms. In online learning, at each timestep $t \in [1, 2, \cdots T]$, the network generates an output $\hat{\mathbf{z}}_t^i$ which should match the target trajectory state $\mathbf{z}_t{}^i$. Given M target trajectories: $\mathbf{z}_T^i, i \in [1, 2, \cdots M]$, the objective is to minimize prediction error between network outputs and target states.
We note, our NEF approach can be modified for such a setting via online recursive updates to the weight vector $\mathbf{n}$. This translates to a recursive least-squares (RLS) optimization scheme (SI-Algorithm 1 summarizes our implementation).

Comparison: To evaluate the performance of our method in online learning settings, we compare against two widely-used training algorithms for RNNs: FORCE learning[9, 10] and BP. Each baseline is a trajectory-tracking framework, where the goal is to learn vector field dynamics from simulated low-dimensional trajectories.

We first evaluate on the classical sine wave generation task, originally used to benchmark FORCE [9]. Our rank-2 networks, with targets comprising both the sine signal and its cumulative integral, consistently outperform FORCE-trained full-rank networks (weights were drawn from $\mathcal{N}(0, \frac{1}{d})$) across all tested network sizes (Fig. 3. **A**). Notably, our approach achieves lower MSE while requiring fewer neurons than FORCE, which needs larger networks to suppress chaotic activity to accurately reproduce oscillatory dynamics (for additional comparisons with FORCE see SI E.3).

We next evaluate on a binary decision-making task modeled by a bistable attractor ODE. Both our method and networks trained with BP, learn from teacher trajectories that start at random initial

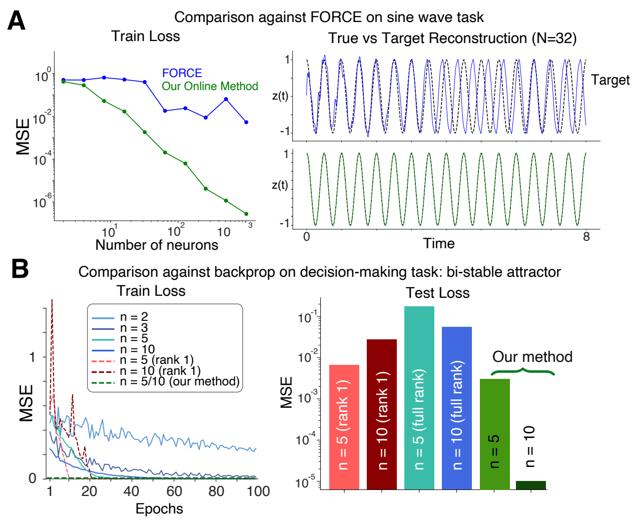

Figure 3: (**A**) Training error as a function of network size for RNNs trained via FORCE and our method on the sine-wave task. Right panel shows qualitative reconstruction for a network with 32 neurons. (**B**) Train and test error for RNNs trained to perform a binary decision-making task using bi-stable attractor dynamics [38, 39].

conditions and converge to one of two fixed points (training details: SI E). As shown in Figure 3.**B**, our approach achieves lower test error across comparable network sizes than both full-rank and low-rank BP-trained networks. Furthermore, our RLS-based approach converges with substantially reduced training time. These results highlight the efficiency of our framework for capturing structured low-dimensional dynamics.

5 Finding the smallest RNN for a given dynamical system

Thus far, we've introduced both offline and online methods for fitting low-rank RNNs to target dynamics, assuming access to a predefined set of nonlinear basis functions. This naturally leads to a fundamental question: *how should this basis set be chosen*? Equivalently, what is the minimal network size required to accurately approximate a given dynamical system? To address this, we now return to the offline setting, where the full target dynamics $g(\mathbf{z})$ are known in advance and $\mathbf{z}$ is a scalar. Our goal is to identify the smallest low-rank RNN—i.e., the minimal number of neurons $d' \ll d$, that can accurately implement the function $g(\mathbf{z})$. Formally, we pose this as a sparse approximation problem: find a minimal subset of basis functions $\Phi(\mathbf{m}, \mathbf{b})$ and corresponding weights $\mathbf{n}$ such that the network can faithfully reproduce the dynamics. Mathematically, this implies selecting the best d' entries from $\Phi(\mathbf{m}, \mathbf{b})$, to create a basis:

$$\Phi_{d'}(\mathbf{m}, \mathbf{b}) = \begin{bmatrix} \phi(m_{i_1}\mathbf{z} + \mathbf{b}_{i_1}) \\ \vdots \\ \phi(m_{i_{d'}}\mathbf{z} + \mathbf{b}_{i_{d'}}) \end{bmatrix}, \quad \text{where } \{i_1, \ldots, i_{d'}\} \subseteq \{1, 2, \ldots, d\}.$$

Then, a linear weighting $[n_0 \ \mathbf{n}']$ is learned using least squares regression, where:

$$g(\mathbf{z}) \ \approx \ -n_0 * z + \mathbf{n}'^{\top} \Phi_{d'}(\mathbf{m}, I) \quad \text{where } \{\mathbf{n}' = 1 \times d' \text{ vector}\} \tag{11}$$

To achieve the desired optimization of approximating $g(\mathbf{z})$, we begin with a large enough $\Phi(\mathbf{m}, \mathbf{b})$ obtained by sampling from a uniform grid of values for $(\mathbf{m}, \mathbf{b})$. We then follow an iterative approach, wherein at each iteration t, we greedily pick a basis function i_j with the highest alignment to the current residual estimate of $g(\mathbf{z})$. This is done via an adaptation of the well-established orthogonal matching pursuit (OMP) framework. A more detailed description of this process is provided in SI-Algorithm 2.

It is worth noting, changing the original basis set $\Phi(\mathbf{m}, \mathbf{b})$ to $\Phi'(\mathbf{m}, \mathbf{b})$, could result in the algorithm converging to a different minima (global minima in $\Phi'(\mathbf{m}, \mathbf{b})$ could be different from global minima in $\Phi(\mathbf{m}, \mathbf{b})$). However, if the basis sets are equivalent, we observe similar performance across simulations (SI- Fig 13)).

We also introduce a continuous extension of this framework [40, 41]. Unlike standard OMP, which selects from a discrete set of basis functions, continuous-OMP refines each selected basis function by

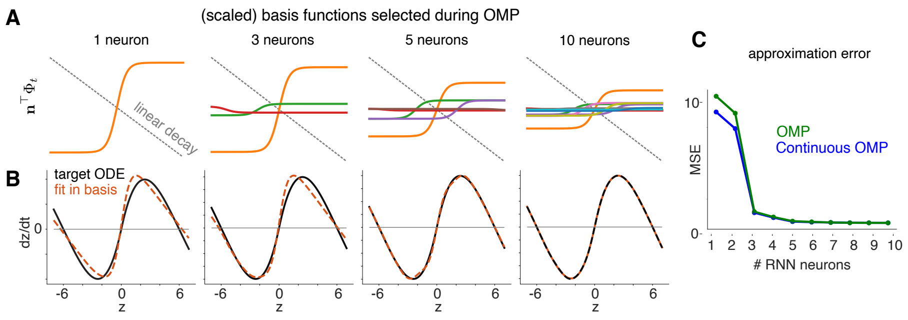

Figure 4: Finding the smallest RNN for a particular nonlinear dynamical system using orthogonal matching pursuit (OMP). **(A)** Scaled basis functions selected after $1, 3, 5$, and 10 iterations of OMP, along with the linear decay term $-z$ for an example ODE (shown below). **(B)** Target ODE (black) and RNN fit after each step of OMP. **(C)** Mean squared error (MSE) between target ODE and RNN approximation as a function of the number of RNN neurons added by OMP, and our continuous OMP (COMP) method.

optimizing its parameters. Specifically, after each greedy selection, we optimize the corresponding $(\mathbf{m}, \mathbf{b})$ values by performing gradient descent on the ordinary least-squares objective (Eqn 11). Thus we search a continuous space of basis functions rather than being limited to a predefined discrete set, offering greater flexibility in finding the optimal representation of $g(\mathbf{z})$.

In Fig 4, we apply this method to a simulated 1D ODE, with two stable fixed points and one unstable fixed point. The first row shows the greedily-added basis functions, multiplied by their corresponding learned linear weightings. The bottom row shows their linear combination against the true underlying ODE. Through this iterative process, we observe with just 5 neurons our network almost perfectly reconstructs the target ODE. Finally, we note our COMP method of optimization allows for fine-tuning of the basis functions' parameters, therefore leading to more accurate approximations with fewer neurons (Fig. 4C shows sharper drops in MSE for fewer neurons). We also apply this method to higher dimensional dynamics (SI D).

Critically, previous work (e.g., [39, 17]) have similar dynamics which are learned using BP with much larger networks (typically 512 neurons). Our method instead provides an empirical framework to find the minimum number of neurons needed to fit dynamics within estimated margins of error.

6 Infinite low-rank RNNs

So far we have taken a "primal space" view of fitting low-rank RNNs, in which we optimize the linear weights N over a fixed nonlinear basis in order to fit a dynamical system of interest. In this section we will instead rely on a dual space view in order to optimize the distribution of nonlinear basis functions employed in this representation. This view will in turn allow us to consider low-rank RNNs where the number of units goes to infinity.

For simplicity, we focus on a rank–1 network with constant filtered input $(\mathbf{v})$ given by:

$$g(z) = \sum_{i=1}^{d} \mathbf{n}_i \, \phi(\mathbf{m}_i z + \mathbf{b}_i \mathbf{v}) \tag{12}$$

Rather than fixing d and optimizing the parameters $\{\mathbf{n}, \mathbf{m}, \mathbf{b}\}$ directly as we've done previously, in this section we instead take a *bayesian perspective* by placing prior distributions over the network weights. This in turn also makes $g(z)$ a random variable, through which we can then characterize the distribution over functions expressible by the network. More precisely, instead of solving the regression problem in the primal form (Eqn 8), the dual space view considers the similarity between inputs $\mathbf{z}$ and $\mathbf{z}'$ in feature space denoted by the covariance kernel depicted in Eqn 13.

$$K(z, z') = \mathbb{E}_{(\mathbf{m},\mathbf{b})} \left[\phi(\mathbf{m}^\top \mathbf{z} + \mathbf{b}^\top \mathbf{v}) \, \phi(\mathbf{m}^\top \mathbf{z}' + \mathbf{b}^\top \mathbf{v}) \right] \tag{13}$$

Furthermore, the Central Limit Theorem ensures that in the limit of infinite basis functions (or neurons) $d \to \infty$, the network output converges to a Gaussian Process: $g(z) \xrightarrow{d} GP(0, K)$, thus revealing that an infinitely wide low-rank RNN is *exactly* equivalent to a GP over state dynamics. Additionally, the specific form of the induced kernel is parameterized by the choice of nonlinearity ϕ and the distribution over $(\mathbf{m}, I)$. Specifically, when $\phi = \mathrm{erf}(\cdot)$ and the weights $(m, \mathbf{b}) \sim \mathcal{N}(0, \Sigma)$, we recover the well known arcsin analytic kernel [30, 29, 31]:

$$K_\Sigma(z, z') = \frac{2}{\pi} \sin^{-1}\left(\frac{2\, z^\top \Sigma z'}{\sqrt{(1+2z^\top \Sigma z)\,(1+2z'^\top \Sigma z')}}\right) \tag{14}$$

where the kernel hyperparameters $\Sigma = \{\sigma_m^2, \sigma_b^2, \sigma_{mb}\}$, characterize the distribution of this basis.

Thus, given noisy observations of the form $y_i = g(z_i) + \epsilon$, with $\epsilon \sim \mathcal{N}(0, \sigma_n^2)$, we perform GP regression and maximize the log marginal likelihood:

$$\log p(\mathbf{y} \mid \mathbf{z}, \Sigma) = -\tfrac{1}{2}\mathbf{y}^\top (K_\Sigma + \sigma_n^2 I)^{-1}\mathbf{y} - \tfrac{1}{2}\log \left\| K_\Sigma + \sigma_n^2 I \right\| - \tfrac{N}{2}\log 2\pi.$$

Optimizing this objective over Σ selects a basis distribution that is statistically aligned with the data. Figure 5 compares GP regression fits under two such choices. Panel **A** shows the result using a standard normal prior over $(\mathbf{m}, \mathbf{b})$, as is common in the literature [3, 16, 6, 17]; the fit is poor and uncertainty remains high, especially away from the training points. Panel **B** shows the result after optimizing Σ: the posterior mean better matches the target function, and uncertainty is markedly reduced. This improvement stems from a data-adaptive kernel matrix that more faithfully captures the structure of the underlying dynamics. Finally, we train *finite rank*-1 *networks* using backprop-through-time (BPTT) and our online method (RLS) on trajectories generated from the ODE depicted in Panels A and B. We demonstrate that in both cases, GP-optimized bases yield lower training MSE than standard-normal bases (Panel C). These findings represent averages over 5 seeds of initialization; for additional training details see SI E.2.

Together, these results underscore the sensitivity of low-rank models to their initialization and show how a principled, inference-based approach can mitigate this sensitivity without relying on extensive trial and error.

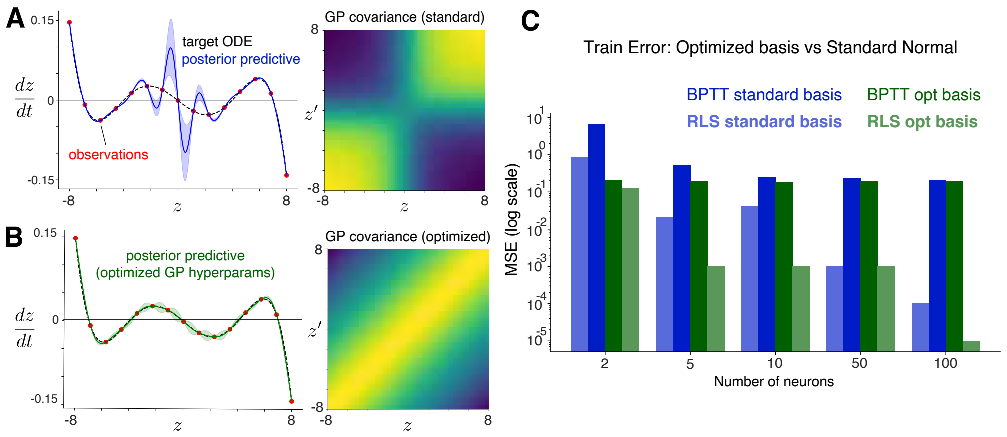

Figure 5: **Low-rank RNN as a Gaussian process.** (**A**) Targed ODE and posterior predictive distribution for an infinite RNN given a set of observations (red small). Here the GP covariance function (right) assumes a standard normal prior over basis parameters $\mathbf{m}$ and $\mathbf{b}$. (**B**) Infinite RNN predictive distribution with optimized GP covariance hyperparameters (values obtained: $\sigma_m^2 = 0.6, \sigma_b^2 = 4.5, \sigma_{mb} = 0.01$), and resulting GP covariance (right). (**C**) Comparison of networks trained by initialization from optimal basis distribution vs the standard normal distribution. Rank 1 networks trained with BPTT & our online method (RLS) achieve lower train MSE. Standard basis implies network parameters were initialized via standard normal distributions. Opt basis corresponds to intializing network weights with the GP found hyper-parameters.

7 Active learning for low-rank RNNs

Another consequence of the dual space view is that it naturally suggests an *active learning* strategy for sample-efficient fitting of low-rank RNNs. That is, if we can measure the ODE at a limited number of locations in latent space $\mathbf{z}$ and input space $\mathbf{v}$, where should we take those measurements? Here we build on previous work on adaptive experimental design that proposed selecting inputs that maximize information gain about the parameters of interest [42–45]. If we assume independent Gaussian noise in our measurements of $d\mathbf{z}/dt$, then the maximally informative location $(\mathbf{z}, \mathbf{v})$ is the one that maximizes our uncertainty about the weights $\mathbf{n}$, which in turn corresponds to the maximal eigenvector of the posterior covariance.

Given the design matrix $\Phi = \phi(\mathbf{m}\mathbf{z} + \mathbf{b}\mathbf{v})$ and target vector $\mathbf{y} = g(\mathbf{z}) + \mathbf{z}$, the posterior covariance over $\mathbf{n}$ under a Gaussian prior is proportional to:

$$\mathbf{\Sigma} = (\Phi^\top \Phi + \lambda I)^{-1}, \tag{15}$$

where λ is the ratio of measurement noise variance to prior variance. For a candidate data-point (z, v) the predictive distribution is Gaussian with variance:

$$\sigma^2(z, v) \;=\; \phi(\mathbf{m}z + \mathbf{b}v)^\top \mathbf{\Sigma}\, \phi(\mathbf{m}z + \mathbf{b}v) \tag{16}$$

The most informative point for the next trial is the maximizer of the predictive variance:

$$(z^\star, v^\star) \;=\; \underset{(z,v)\in\Phi}{\arg\max}\; \phi(\mathbf{m}z + \mathbf{b}v)^\top \big(\Phi^\top \Phi + \lambda I\big)^{-1} \phi(\mathbf{m}z + \mathbf{b}v), \tag{17}$$

which corresponds to the point in (z, v) space with maximal projection onto the top eigenvector of $\mathbf{\Sigma}$. Intuitively, (17) targets regions where current uncertainty is maximal, therefore yielding the highest expected information gain per data point. Each selected point is added to the dataset, and the linear weight $\mathbf{n}$, is updated using the posterior mean given the data collected so far.

We illustrate this process in Fig. 6 for a system with non-normal dynamics. The heat map represents $\sigma^2(z, v)$, while red arrows depict the estimated vector field after each active data acquisition. Initially, uncertainty is highest in unexplored regions (yellow); as more samples are acquired, the learned dynamics converge rapidly to the true ODE. Furthermore, it is worth noting that within this setting we can also compute the *minimum number of samples* required to obtain a desired MSE; this bound depends on the dimensionality of the kernel function over the support of our system (i.e., the eigenspectrum of $\Phi^\top \Phi$ over a grid of $z, v \in [-1, +1]$), and the level of observational noise [46].

In conclusion, by exploiting the closed-form posterior in the dual (kernel) space, we obtain a computationally efficient and statistically grounded acquisition rule that significantly reduces the number of samples required to fit the system dynamics.

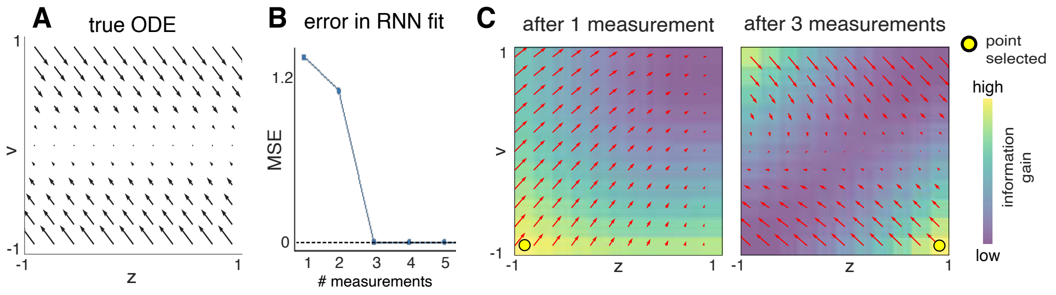

Figure 6: **Active learning for low-rank RNNs.** **(A)** Target ODE flow field over latent z and input v, reflecting non-normal dynamics. **(B)** Mean squared error of rank-1 RNN approximation as a function of the number of active learning measurements. **(C)** Fitted ODE (red arrows) after 1 (left) and 3 (right) measurements selected using active learning. Heatmap shows the predictive variance (heatmap) used to compute the most informative point for the next trial (yellow dot).

8 Discussion

In this paper we have introduced several novel methods for low-rank RNNs, including: (1) an online learning rule for training RNNs that substantially outperforms FORCE and backprop; (2)

methods for finding minimal RNNs (i.e., RNNs with the fewest units) using an extension of OMP; (3) infinite low-rank RNNs using the equivalent Gaussian Process; and (4) active learning methods for identifying the most informative points in state space to quickly learn an approximation to an ODE of interest. Note that the third contribution provides a novel solution to the problem of optimizing the nonlinear basis functions, that is, optimizing the distribution over M and B parameters so that the model can accurately implement an ODE of interest. We propose maximum marginal likelihood of the equivalent GP kernel hyperparameters can thus be used to obtain improved initializations for low-rank RNNs, even in finite models that are ultimately trained with gradient based methods.

These results also open up several promising directions for future work. We have focused on the problem of embedding an ODE of interest; an important related problem is to infer low-rank networks underlying high-dimensional neural observations, a problem recently considered in [37]. Second, our active learning method assumed the ability to sample arbitrary locations in latent space, which is unrealistic in practice. A promising future direction is to develop control theoretic methods to find maximally informative inputs to the system [44]. Finally, we examined GPs equivalent to infinite RNNs for specific choices of nonlinearity (namely erf, which we explored here, or ReLU [47]), but designing kernels that best approximate the data and then extending these kernel functions to closed-form analytic solutions remains an open problem [48].

Altogether, our contributions establish a theoretical and practical foundation for designing interpretable and sample-efficient low-rank RNNs, with broad applicability in both machine learning and neuroscience.

References

[1] Paul Miller, Carlos D Brody, Ranulfo Romo, and Xiao-Jing Wang. A recurrent network model of somatosensory parametric working memory in the prefrontal cortex. *Cerebral Cortex*, 13(11):1208–1218, 2003.

[2] Omri Barak. Recurrent neural networks as versatile tools of neuroscience research. *Current opinion in neurobiology*, 46:1–6, 2017.

[3] Francesca Mastrogiuseppe and Srdjan Ostojic. Linking connectivity, dynamics, and computations in low-rank recurrent neural networks. *Neuron*, 99(3):609–623, 2018.

[4] R. Schaeffer, M. Khona, L. Meshulam, International Brain Laboratory, and Ila R. Fiete. Reverse-engineering recurrent neural network solutions to a hierarchical inference task for mice. *bioRxiv*, pages 2020–06, 2020.

[5] Lea Duncker and Maneesh Sahani. Dynamics on the manifold: Identifying computational dynamical activity from neural population recordings. *Current opinion in neurobiology*, 70:163–170, 2021.

[6] Alexis Dubreuil, Adrian Valente, Manuel Beiran, Francesca Mastrogiuseppe, and Srdjan Ostojic. The role of population structure in computations through neural dynamics. *Nature neuroscience*, 25(6):783–794, 2022.

[7] Herbert Jaeger. The "echo state" approach to analysing and training recurrent neural networks. *Bonn, Germany: German National Research Center for Information Technology GMD Technical Report*, 148:34, 2001.

[8] Wolfgang Maass, Thomas Natschläger, and Henry Markram. Real-time computing without stable states: A new framework for neural computation based on perturbations. *Neural Computation*, 14:2531–2560, 2002.

[9] David Sussillo and L. F. Abbott. Generating coherent patterns of activity from chaotic neural networks. *Neuron*, 63(4):544–557, Aug 2009. doi: 10.1016/j.neuron.2009.07.018. URL `http://dx.doi.org/10.1016/j.neuron.2009.07.018`.

[10] Brian DePasquale, Christopher J. Cueva, Kanaka Rajan, G. Sean Escola, and L. F. Abbott. full-force: A target-based method for training recurrent networks. *PLOS ONE*, 13(2):1–18, 02 2018. doi: 10.1371/journal.pone.0191527. URL `https://doi.org/10.1371/journal.pone.0191527`.

[11] Barak A Pearlmutter. Dynamic recurrent neural networks. 1990.

[12] David Sussillo and Omri Barak. Opening the black box: low-dimensional dynamics in high-dimensional recurrent neural networks. *Neural computation*, 25(3):626–649, 2013.

[13] Timothy P Lillicrap and Adam Santoro. Backpropagation through time and the brain. *Current opinion in neurobiology*, 55:82–89, 2019.

[14] Valerio Mante, David Sussillo, Krishna V Shenoy, and William T Newsome. Context-dependent computation by recurrent dynamics in prefrontal cortex. *Nature*, 503(7474):78–84, 2013.

[15] Alex H Williams, Erin Kunz, Simon Kornblith, and Scott Linderman. Generalized shape metrics on neural representations. *Advances in Neural Information Processing Systems*, 34:4738–4750, 2021.

[16] Manuel Beiran, Alexis Dubreuil, Adrian Valente, Francesca Mastrogiuseppe, and Srdjan Ostojic. Shaping dynamics with multiple populations in low-rank recurrent networks. *Neural Computation*, 33(6):1572–1615, 2021.

[17] Adrian Valente, Jonathan W Pillow, and Srdjan Ostojic. Extracting computational mechanisms from neural data using low-rank rnns. *Advances in Neural Information Processing Systems*, 35:24072–24086, 2022.

[18] Chris Eliasmith and Charles H Anderson. *Neural engineering: Computation, representation, and dynamics in neurobiological systems*. MIT press, 2003.

[19] Terrence C Stewart. A technical overview of the neural engineering framework. *University of Waterloo*, 110, 2012.

[20] Martin Boerlin, Christian K. Machens, and Sophie Denève. Predictive coding of dynamical variables in balanced spiking networks. *PLoS Comput Biol*, 9(11):e1003258, 11 2013. doi: 10.1371/journal.pcbi.1003258. URL `http://dx.doi.org/10.1371%2Fjournal.pcbi.1003258`.

[21] Omri Barak and Sandro Romani. Mapping low-dimensional dynamics to high-dimensional neural activity: A derivation of the ring model from the neural engineering framework. *Neural Computation*, 33(3): 827–852, 2021.

[22] Larry F Abbott, Brian DePasquale, and Raoul-Martin Memmesheimer. Building functional networks of spiking model neurons. *Nature neuroscience*, 19(3):350–355, 2016.

[23] Alireza Alemi, Christian Machens, Sophie Deneve, and Jean-Jacques Slotine. Learning nonlinear dynamics in efficient, balanced spiking networks using local plasticity rules. In *Proceedings of the AAAI conference on artificial intelligence*, volume 32, 2018.

[24] Markus Heinonen, Cagatay Yildiz, Henrik Mannerström, Jukka Intosalmi, and Harri Lähdesmäki. Learning unknown ode models with gaussian processes. In *International conference on machine learning*, pages 1959–1968. PMLR, 2018.

[25] Harish S Bhat, Majerle Reeves, and Ramin Raziperchikolaei. Estimating vector fields from noisy time series. In *2020 54th Asilomar Conference on Signals, Systems, and Computers*, pages 599–606. IEEE, 2020.

[26] Steven L Brunton, Joshua L Proctor, and J Nathan Kutz. Sparse identification of nonlinear dynamics with control (sindyc). *IFAC-PapersOnLine*, 49(18):710–715, 2016.

[27] Fernando Lejarza and Michael Baldea. Data-driven discovery of the governing equations of dynamical systems via moving horizon optimization. *Scientific reports*, 12(1):11836, 2022.

[28] Manuel Brenner, Florian Hess, Jonas M Mikhaeil, Leonard F Bereska, Zahra Monfared, Po-Chen Kuo, and Daniel Durstewitz. Tractable dendritic rnns for reconstructing nonlinear dynamical systems. In *International conference on machine learning*, pages 2292–2320. Pmlr, 2022.

[29] Christopher Williams. Computing with infinite networks. *Advances in neural information processing systems*, 9, 1996.

[30] Radford M Neal and Radford M Neal. Priors for infinite networks. *Bayesian learning for neural networks*, pages 29–53, 1996.

[31] Jaehoon Lee, Yasaman Bahri, Roman Novak, Samuel S Schoenholz, Jeffrey Pennington, and Jascha Sohl-Dickstein. Deep neural networks as gaussian processes. *arXiv preprint arXiv:1711.00165*, 2017.

[32] Greg Yang. Wide feedforward or recurrent neural networks of any architecture are gaussian processes. *Advances in Neural Information Processing Systems*, 32, 2019.

[33] Greg Yang. Scaling limits of wide neural networks with weight sharing: Gaussian process behavior, gradient independence, and neural tangent kernel derivation. *arXiv preprint arXiv:1902.04760*, 2019.

[34] Xiang Sun, Seongyoon Kim, and Jung-Il Choi. Recurrent neural network-induced gaussian process. *Neurocomputing*, 509:75–84, 2022.

[35] Ricky TQ Chen, Yulia Rubanova, Jesse Bettencourt, and David K Duvenaud. Neural ordinary differential equations. *Advances in neural information processing systems*, 31, 2018.

[36] Arthur Pellegrino, N Alex Cayco Gajic, and Angus Chadwick. Low tensor rank learning of neural dynamics. *Advances in Neural Information Processing Systems*, 36:11674–11702, 2023.

[37] Matthijs Pals, A Erdem Sagtekin, Felix Pei, Manuel Gloeckler, and Jakob H Macke. Inferring stochastic low-rank recurrent neural networks from neural data. arxiv [cs. lg], 2024.

[38] Kong-Fatt Wong and Xiao-Jing Wang. A recurrent network mechanism of time integration in perceptual decisions. *Journal of Neuroscience*, 26(4):1314–1328, 2006.

[39] Thomas Zhihao Luo, Timothy Doyeon Kim, Diksha Gupta, Adrian G Bondy, Charles D Kopec, Verity A Elliot, Brian DePasquale, and Carlos D Brody. Transitions in dynamical regime and neural mode underlie perceptual decision-making. *bioRxiv*, pages 2023–10, 2023.

[40] Chaitanya Ekanadham, Daniel Tranchina, and Eero P Simoncelli. Recovery of sparse translation-invariant signals with continuous basis pursuit. *IEEE transactions on signal processing*, 59(10):4735–4744, 2011.

[41] Karin C Knudson, Jacob Yates, Alexander Huk, and Jonathan W Pillow. Inferring sparse representations of continuous signals with continuous orthogonal matching pursuit. *Advances in neural information processing systems*, 27, 2014.

[42] David J.C. MacKay. Information-based objective functions for active data selection. *Neural Computation*, 4(4):590–604, 1992.

[43] Hendrik Kuck, Nando de Freitas, and Arnaud Doucet. Smc samplers for bayesian optimal nonlinear design. In *2006 IEEE Nonlinear Statistical Signal Processing Workshop*, pages 99–102. IEEE, 2006.

[44] Horia Mania, Michael I. Jordan, and Benjamin Recht. Active learning for nonlinear system identification with guarantees. *Journal of Machine Learning Research*, 23(32):1–30, 2022. URL `http://jmlr.org/papers/v23/20-807.html`.

[45] Aditi Jha, Zoe C Ashwood, and Jonathan W Pillow. Active learning for discrete latent variable models. *Neural computation*, 36(3):437–474, 2024.

[46] Kathryn Chaloner and Isabella Verdinelli. Bayesian experimental design: A review. *Statistical science*, pages 273–304, 1995.

[47] Youngmin Cho and Lawrence Saul. Kernel methods for deep learning. *Advances in neural information processing systems*, 22, 2009.

[48] James Benjamin Simon, Sajant Anand, and Mike Deweese. Reverse engineering the neural tangent kernel. In *International Conference on Machine Learning*, pages 20215–20231. PMLR, 2022.

NeurIPS Paper Checklist

The checklist is designed to encourage best practices for responsible machine learning research, addressing issues of reproducibility, transparency, research ethics, and societal impact. Do not remove the checklist: **The papers not including the checklist will be desk rejected.** The checklist should follow the references and precede the (optional) supplemental material. The checklist does NOT count towards the page limit.

Please read the checklist guidelines carefully for information on how to answer these questions. For each question in the checklist:

- You should answer [Yes] , [No] , or [NA] .
- [NA] means either that the question is Not Applicable for that particular paper or the relevant information is Not Available.
- Please provide a short (1–2 sentence) justification right after your answer (even for NA).

The checklist answers are an integral part of your paper submission. They are visible to the reviewers, area chairs, senior area chairs, and ethics reviewers. You will be asked to also include it (after eventual revisions) with the final version of your paper, and its final version will be published with the paper.

The reviewers of your paper will be asked to use the checklist as one of the factors in their evaluation. While "[Yes] " is generally preferable to "[No] ", it is perfectly acceptable to answer "[No] " provided a proper justification is given (e.g., "error bars are not reported because it would be too computationally expensive" or "we were unable to find the license for the dataset we used"). In general, answering "[No] " or "[NA] " is not grounds for rejection. While the questions are phrased in a binary way, we acknowledge that the true answer is often more nuanced, so please just use your best judgment and write a justification to elaborate. All supporting evidence can appear either in the main paper or the supplemental material, provided in appendix. If you answer [Yes] to a question, in the justification please point to the section(s) where related material for the question can be found.

IMPORTANT, please:

- **Delete this instruction block, but keep the section heading "NeurIPS paper checklist"**,
- **Keep the checklist subsection headings, questions/answers and guidelines below.**
- **Do not modify the questions and only use the provided macros for your answers**.

1. **Claims**

   Question: Do the main claims made in the abstract and introduction accurately reflect the paper's contributions and scope?

   Answer: [Yes]

   Justification: We have elaborated on all claims made in the abstract and introduction in the main paper, and they reflect the paper's contributions accurately

   Guidelines:

   - The answer NA means that the abstract and introduction do not include the claims made in the paper.
   - The abstract and/or introduction should clearly state the claims made, including the contributions made in the paper and important assumptions and limitations. A No or NA answer to this question will not be perceived well by the reviewers.
   - The claims made should match theoretical and experimental results, and reflect how much the results can be expected to generalize to other settings.
   - It is fine to include aspirational goals as motivation as long as it is clear that these goals are not attained by the paper.

2. **Limitations**

   Question: Does the paper discuss the limitations of the work performed by the authors?

   Answer: [Yes]

Justification: We discuss limitations in the discussion/conclusion section.

Guidelines:

- The answer NA means that the paper has no limitation while the answer No means that the paper has limitations, but those are not discussed in the paper.
- The authors are encouraged to create a separate "Limitations" section in their paper.
- The paper should point out any strong assumptions and how robust the results are to violations of these assumptions (e.g., independence assumptions, noiseless settings, model well-specification, asymptotic approximations only holding locally). The authors should reflect on how these assumptions might be violated in practice and what the implications would be.
- The authors should reflect on the scope of the claims made, e.g., if the approach was only tested on a few datasets or with a few runs. In general, empirical results often depend on implicit assumptions, which should be articulated.
- The authors should reflect on the factors that influence the performance of the approach. For example, a facial recognition algorithm may perform poorly when image resolution is low or images are taken in low lighting. Or a speech-to-text system might not be used reliably to provide closed captions for online lectures because it fails to handle technical jargon.
- The authors should discuss the computational efficiency of the proposed algorithms and how they scale with dataset size.
- If applicable, the authors should discuss possible limitations of their approach to address problems of privacy and fairness.
- While the authors might fear that complete honesty about limitations might be used by reviewers as grounds for rejection, a worse outcome might be that reviewers discover limitations that aren't acknowledged in the paper. The authors should use their best judgment and recognize that individual actions in favor of transparency play an important role in developing norms that preserve the integrity of the community. Reviewers will be specifically instructed to not penalize honesty concerning limitations.

3. **Theory Assumptions and Proofs**

   Question: For each theoretical result, does the paper provide the full set of assumptions and a complete (and correct) proof?

   Answer:[NA] .

   Justification: We do not have any theorems or lemmas, as this is not a theory paper

   Guidelines:

   - The answer NA means that the paper does not include theoretical results.
   - All the theorems, formulas, and proofs in the paper should be numbered and cross-referenced.
   - All assumptions should be clearly stated or referenced in the statement of any theorems.
   - The proofs can either appear in the main paper or the supplemental material, but if they appear in the supplemental material, the authors are encouraged to provide a short proof sketch to provide intuition.
   - Inversely, any informal proof provided in the core of the paper should be complemented by formal proofs provided in appendix or supplemental material.
   - Theorems and Lemmas that the proof relies upon should be properly referenced.

4. **Experimental Result Reproducibility**

   Question: Does the paper fully disclose all the information needed to reproduce the main experimental results of the paper to the extent that it affects the main claims and/or conclusions of the paper (regardless of whether the code and data are provided or not)?

   Answer: [Yes]

   Justification: We have provided details of all parameters and modeling details in the main paper.

   Guidelines:

- The answer NA means that the paper does not include experiments.
- If the paper includes experiments, a No answer to this question will not be perceived well by the reviewers: Making the paper reproducible is important, regardless of whether the code and data are provided or not.
- If the contribution is a dataset and/or model, the authors should describe the steps taken to make their results reproducible or verifiable.
- Depending on the contribution, reproducibility can be accomplished in various ways. For example, if the contribution is a novel architecture, describing the architecture fully might suffice, or if the contribution is a specific model and empirical evaluation, it may be necessary to either make it possible for others to replicate the model with the same dataset, or provide access to the model. In general. releasing code and data is often one good way to accomplish this, but reproducibility can also be provided via detailed instructions for how to replicate the results, access to a hosted model (e.g., in the case of a large language model), releasing of a model checkpoint, or other means that are appropriate to the research performed.
- While NeurIPS does not require releasing code, the conference does require all submissions to provide some reasonable avenue for reproducibility, which may depend on the nature of the contribution. For example
  (a) If the contribution is primarily a new algorithm, the paper should make it clear how to reproduce that algorithm.
  (b) If the contribution is primarily a new model architecture, the paper should describe the architecture clearly and fully.
  (c) If the contribution is a new model (e.g., a large language model), then there should either be a way to access this model for reproducing the results or a way to reproduce the model (e.g., with an open-source dataset or instructions for how to construct the dataset).
  (d) We recognize that reproducibility may be tricky in some cases, in which case authors are welcome to describe the particular way they provide for reproducibility. In the case of closed-source models, it may be that access to the model is limited in some way (e.g., to registered users), but it should be possible for other researchers to have some path to reproducing or verifying the results.

5. **Open access to data and code**

   Question: Does the paper provide open access to the data and code, with sufficient instructions to faithfully reproduce the main experimental results, as described in supplemental material?

   Answer: [No]

   Justification: We will release code with the final version of the manuscript. However, we provide sufficient details to replicate our framework.

   Guidelines:

   - The answer NA means that paper does not include experiments requiring code.
   - Please see the NeurIPS code and data submission guidelines (`https://nips.cc/public/guides/CodeSubmissionPolicy`) for more details.
   - While we encourage the release of code and data, we understand that this might not be possible, so "No" is an acceptable answer. Papers cannot be rejected simply for not including code, unless this is central to the contribution (e.g., for a new open-source benchmark).
   - The instructions should contain the exact command and environment needed to run to reproduce the results. See the NeurIPS code and data submission guidelines (`https://nips.cc/public/guides/CodeSubmissionPolicy`) for more details.
   - The authors should provide instructions on data access and preparation, including how to access the raw data, preprocessed data, intermediate data, and generated data, etc.
   - The authors should provide scripts to reproduce all experimental results for the new proposed method and baselines. If only a subset of experiments are reproducible, they should state which ones are omitted from the script and why.

- At submission time, to preserve anonymity, the authors should release anonymized versions (if applicable).
- Providing as much information as possible in supplemental material (appended to the paper) is recommended, but including URLs to data and code is permitted.

6. **Experimental Setting/Details**

   Question: Does the paper specify all the training and test details (e.g., data splits, hyperparameters, how they were chosen, type of optimizer, etc.) necessary to understand the results?

   Answer: [Yes]

   Justification: Our paper focuses on a closed form solution via regression and are reproduce using the classical ridge regression solution, thereby not requiring any specific error bars/solvers. We provide details on initial conditions which allow reproducing our results. Additionally, for networks trained via BP we provide necessary details on the task and data used, with additional training details (epochs trained etc) in the supplement.

   Guidelines:

   - The answer NA means that the paper does not include experiments.
   - The experimental setting should be presented in the core of the paper to a level of detail that is necessary to appreciate the results and make sense of them.
   - The full details can be provided either with the code, in appendix, or as supplemental material.

7. **Experiment Statistical Significance**

   Question: Does the paper report error bars suitably and correctly defined or other appropriate information about the statistical significance of the experiments?

   Answer: [Yes]

   Justification: Our paper focuses on a closed form solution via regression and are reproduce using the classical ridge regression solution, thereby not requiring any specific error bars/solvers. We provide details on initial conditions which allow reproducing our results.

   Guidelines:

   - The answer NA means that the paper does not include experiments.
   - The authors should answer "Yes" if the results are accompanied by error bars, confidence intervals, or statistical significance tests, at least for the experiments that support the main claims of the paper.
   - The factors of variability that the error bars are capturing should be clearly stated (for example, train/test split, initialization, random drawing of some parameter, or overall run with given experimental conditions).
   - The method for calculating the error bars should be explained (closed form formula, call to a library function, bootstrap, etc.)
   - The assumptions made should be given (e.g., Normally distributed errors).
   - It should be clear whether the error bar is the standard deviation or the standard error of the mean.
   - It is OK to report 1-sigma error bars, but one should state it. The authors should preferably report a 2-sigma error bar than state that they have a 96% CI, if the hypothesis of Normality of errors is not verified.
   - For asymmetric distributions, the authors should be careful not to show in tables or figures symmetric error bars that would yield results that are out of range (e.g. negative error rates).
   - If error bars are reported in tables or plots, The authors should explain in the text how they were calculated and reference the corresponding figures or tables in the text.

8. **Experiments Compute Resources**

   Question: For each experiment, does the paper provide sufficient information on the computer resources (type of compute workers, memory, time of execution) needed to reproduce the experiments?

Answer: [Yes]

Justification: We provide details in the main/supplement.

Guidelines:

- The answer NA means that the paper does not include experiments.
- The paper should indicate the type of compute workers CPU or GPU, internal cluster, or cloud provider, including relevant memory and storage.
- The paper should provide the amount of compute required for each of the individual experimental runs as well as estimate the total compute.
- The paper should disclose whether the full research project required more compute than the experiments reported in the paper (e.g., preliminary or failed experiments that didn't make it into the paper).

9. **Code Of Ethics**

   Question: Does the research conducted in the paper conform, in every respect, with the NeurIPS Code of Ethics `https://neurips.cc/public/EthicsGuidelines`?

   Answer: [Yes]

   Justification: This paper adheres to the NeurIPS code of conduct.

   Guidelines:

   - The answer NA means that the authors have not reviewed the NeurIPS Code of Ethics.
   - If the authors answer No, they should explain the special circumstances that require a deviation from the Code of Ethics.
   - The authors should make sure to preserve anonymity (e.g., if there is a special consideration due to laws or regulations in their jurisdiction).

10. **Broader Impacts**

    Question: Does the paper discuss both potential positive societal impacts and negative societal impacts of the work performed?

    Answer: [NA]

    Justification: We do not envision any societal impact of this work

    Guidelines:

    - The answer NA means that there is no societal impact of the work performed.
    - If the authors answer NA or No, they should explain why their work has no societal impact or why the paper does not address societal impact.
    - Examples of negative societal impacts include potential malicious or unintended uses (e.g., disinformation, generating fake profiles, surveillance), fairness considerations (e.g., deployment of technologies that could make decisions that unfairly impact specific groups), privacy considerations, and security considerations.
    - The conference expects that many papers will be foundational research and not tied to particular applications, let alone deployments. However, if there is a direct path to any negative applications, the authors should point it out. For example, it is legitimate to point out that an improvement in the quality of generative models could be used to generate deepfakes for disinformation. On the other hand, it is not needed to point out that a generic algorithm for optimizing neural networks could enable people to train models that generate Deepfakes faster.
    - The authors should consider possible harms that could arise when the technology is being used as intended and functioning correctly, harms that could arise when the technology is being used as intended but gives incorrect results, and harms following from (intentional or unintentional) misuse of the technology.
    - If there are negative societal impacts, the authors could also discuss possible mitigation strategies (e.g., gated release of models, providing defenses in addition to attacks, mechanisms for monitoring misuse, mechanisms to monitor how a system learns from feedback over time, improving the efficiency and accessibility of ML).

11. **Safeguards**

Question: Does the paper describe safeguards that have been put in place for responsible release of data or models that have a high risk for misuse (e.g., pretrained language models, image generators, or scraped datasets)?

Answer: [NA]

Justification: The paper poses no such risks.

Guidelines:

- The answer NA means that the paper poses no such risks.
- Released models that have a high risk for misuse or dual-use should be released with necessary safeguards to allow for controlled use of the model, for example by requiring that users adhere to usage guidelines or restrictions to access the model or implementing safety filters.
- Datasets that have been scraped from the Internet could pose safety risks. The authors should describe how they avoided releasing unsafe images.
- We recognize that providing effective safeguards is challenging, and many papers do not require this, but we encourage authors to take this into account and make a best faith effort.

12. **Licenses for existing assets**

Question: Are the creators or original owners of assets (e.g., code, data, models), used in the paper, properly credited and are the license and terms of use explicitly mentioned and properly respected?

Answer: [NA]

Justification: The answer NA means that the paper does not use existing assets

Guidelines:

- The answer NA means that the paper does not use existing assets.
- The authors should cite the original paper that produced the code package or dataset.
- The authors should state which version of the asset is used and, if possible, include a URL.
- The name of the license (e.g., CC-BY 4.0) should be included for each asset.
- For scraped data from a particular source (e.g., website), the copyright and terms of service of that source should be provided.
- If assets are released, the license, copyright information, and terms of use in the package should be provided. For popular datasets, `paperswithcode.com/datasets` has curated licenses for some datasets. Their licensing guide can help determine the license of a dataset.
- For existing datasets that are re-packaged, both the original license and the license of the derived asset (if it has changed) should be provided.
- If this information is not available online, the authors are encouraged to reach out to the asset's creators.

13. **New Assets**

Question: Are new assets introduced in the paper well documented and is the documentation provided alongside the assets?

Answer: [Yes]

Justification: The answer NA means that the paper does not use new assets

Guidelines:

- The answer NA means that the paper does not release new assets.
- Researchers should communicate the details of the dataset/code/model as part of their submissions via structured templates. This includes details about training, license, limitations, etc.
- The paper should discuss whether and how consent was obtained from people whose asset is used.
- At submission time, remember to anonymize your assets (if applicable). You can either create an anonymized URL or include an anonymized zip file.

14. **Crowdsourcing and Research with Human Subjects**

    Question: For crowdsourcing experiments and research with human subjects, does the paper include the full text of instructions given to participants and screenshots, if applicable, as well as details about compensation (if any)?

    Answer: [NA]

    Justification: The paper does not involve crowdsourcing nor research with human subjects

    Guidelines:

    - The answer NA means that the paper does not involve crowdsourcing nor research with human subjects.
    - Including this information in the supplemental material is fine, but if the main contribution of the paper involves human subjects, then as much detail as possible should be included in the main paper.
    - According to the NeurIPS Code of Ethics, workers involved in data collection, curation, or other labor should be paid at least the minimum wage in the country of the data collector.

15. **Institutional Review Board (IRB) Approvals or Equivalent for Research with Human Subjects**

    Question: Does the paper describe potential risks incurred by study participants, whether such risks were disclosed to the subjects, and whether Institutional Review Board (IRB) approvals (or an equivalent approval/review based on the requirements of your country or institution) were obtained?

    Answer: [NA]

    Justification: The paper does not involve crowdsourcing nor research with human subjects

    Guidelines:

    - The answer NA means that the paper does not involve crowdsourcing nor research with human subjects.
    - Depending on the country in which research is conducted, IRB approval (or equivalent) may be required for any human subjects research. If you obtained IRB approval, you should clearly state this in the paper.
    - We recognize that the procedures for this may vary significantly between institutions and locations, and we expect authors to adhere to the NeurIPS Code of Ethics and the guidelines for their institution.
    - For initial submissions, do not include any information that would break anonymity (if applicable), such as the institution conducting the review.

16. **Declaration of LLM usage**

    Question: Does the paper describe the usage of LLMs if it is an important, original, or non-standard component of the core methods in this research? Note that if the LLM is used only for writing, editing, or formatting purposes and does not impact the core methodology, scientific rigorousness, or originality of the research, declaration is not required.

    Answer: [NA]

    Justification: The core method did not involve LLMS for any important, original or non-standard components.

    Guidelines:

    - The answer NA means that the core method development in this research does not involve LLMs as any important, original, or non-standard components.
    - Please refer to our LLM policy (`https://neurips.cc/Conferences/2025/LLM`) for what should or should not be described.

A Choice of nonlinearity

If we consider a network with a rectified-linear instead of a $\tanh$ nonlinearity, the restrictions on the network's representational capacity in the absence of inputs are even more severe (Fig. 7). In this case, the basis functions are all scaled and axis-flipped *relu* functions that intersect the x axis at $x = 0$. Thus they can only represent piecewise linear functions composed of two pieces with a knot at zero. Adding inputs (or per-neuron biases) allows the network to have universal approximation capabilities.

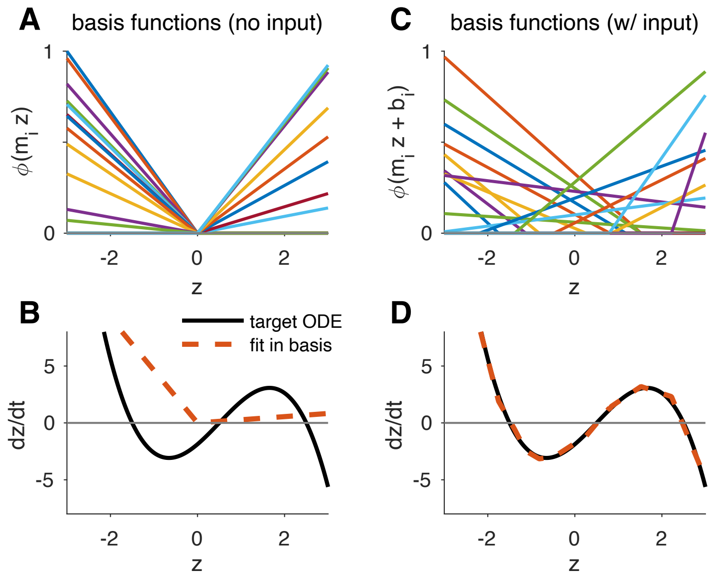

Figure 7: Representational capacity of a 1D low-rank RNN with rectified-linear (*relu*) nonlinearity. **(A)** Set of basis functions obtained by taking random coeffients $m_i \sim \mathcal{N}(0, 1)$ but without input ($\mathbf{v}_t = 0$). **(B)** Attempting to fit an example ODE using this basis recovers only a piecewise linear fit with a kink at zero. **(C)** By adding inputs, basis functions have random offset as well as slope. Here we set $\mathbf{v}_t = 1$ and sampled the input vector coefficients $\mathbf{b}_i \sim \mathcal{N}(0, 1)$. **(D)** Least squares fitting of $\mathbf{n}$ in the random basis from (C) provides a high-accuracy approximation to the target ODE.

A.1 Comparison of activation functions in estimating ODEs

In this section, we explore the low-rank RNN's ability to approximate different types of dynamics (i.e function classes), with different activation functions (i.e basis functions). Our discussion above highlights how relu units can approximate functions through piecewise linear components. Non-zero inputs create basis functions which can be used to compose ODEs with "knots" at the shifted offsets. Alternatively, through our discussion in Section 3, we note tanh units provide smooth non-linear basis functions. The non-zero inputs create shifted basis functions, which perform a similar role, with smooth compositions. Following this intuition, if an ODE consists of smooth non-linear components it can be hypothesized that tanh units would have higher performance. Whereas, if the ODE consists of piecewise linear dynamics, relu units would prove to be more optimal. To validate this, we simulate two such ODEs in Fig. 8. Trivially, in the case of large enough number of basis functions, networks comprising of relu or tanh units can approximate any function (i.e they behave as universal approximators). However, to assess performance, we estimate the smallest networks in both cases that can fit the ODE within a pre-defined margin of error. As expected, the ODE with smoother non-linearities can be fit with smaller tanh networks than relu networks (the opposite is true for piecewise linear ODEs).

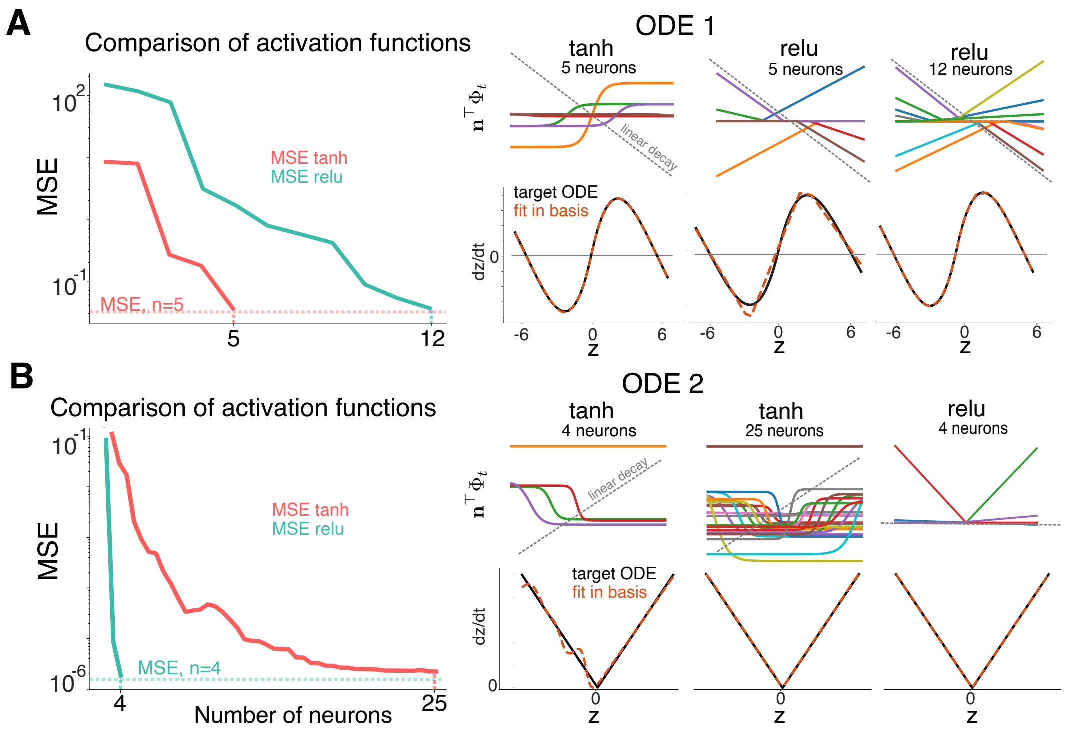

Figure 8: Performance comparison of tanh v/s relu in approximating different ODEs. **(A)** Depicts an ODE with two stable fixed points and one unstable fixed points (better fit with a tanh non-linearity). **(B)** Depicts an ODE with a shifted knot and two linear components (better fit with a RELU non-linearity). First column represents MSE (for a network with tanh and relu activations) as a function of the number of neurons in network. Neurons are added using OMP. The top row of the right column shows scaled basis functions selected via OMP. The bottom row shows fits (orange) of the target ODE (black) at the marked iterations of OMP.

A.2 Absence of inputs for limit cycle

Section 3.1 depicts a limit cycle embedded into the low-rank RNN using our framework. The specific ODE of our non-linear and non-symmetric system is give as -

$$\frac{dx}{dt} = \left(\frac{1-\left(z_0^2+z_1^2\right)}{\sqrt{z_0^2+z_1^2+\epsilon}}\right) z_0 - z_1 - 0.35$$

$$\frac{dy}{dt} = \left(\frac{1-\left(z_0^2+z_1^2\right)}{\sqrt{z_0^2+z_1^2+\epsilon}}\right) z_1 + z_0 + 0.5$$

where ϵ is a small constant added for numerical stability. The constant values in each dimension make the underlying ODE non odd-symmetric.

In this section we show the inability of an RNN without inputs to appropriately approximate this function. In Fig. 9, the first column represents contour plots of the target ODE for each dimension. The overlayed vertical and horizontal dashed red lines depict $X = z_1 = 0, Y = z_2 = 0$ respectively. Note, there is a slight (left and upwards) shift in the contour plots, indicating the non-radial symmetry. This is introduced by adding a constant negative decay in z_1 and a positive correction in z_2. The second and third columns represents the fitted ODEs for an RNN with and without inputs respectively. It can be observed the RNN without inputs is unable to create offsets in any dimension, thus failing at recovering the underlying ODE. To further highlight this we simulate a sample trajectory from the polar coordinates of a limit cycle (detailed in Section 3.1) in the last row of Fig. 9. As expected, the low-rank RNN with inputs almost perfectly overlaps the trajectory, unlike the low-rank RNN without inputs.

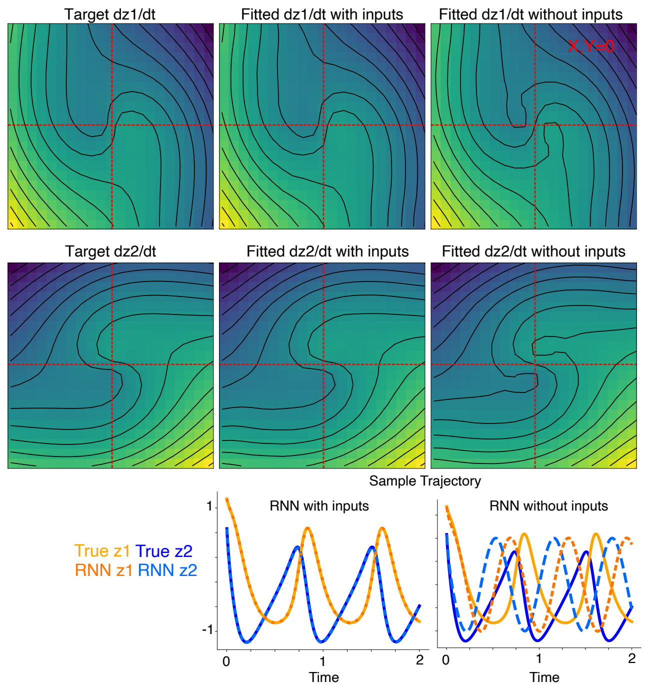

Figure 9: Influence of inputs in capturing non-symmetrical limit cycle

B Online recursive least square (RLS) algorithm

Here we provide additional details on our recursive least-square algorithm. Specifically, for an observed target trajectory $\{\mathbf{z}_t\}_{t=1}^{T}$, with the initial state $\mathbf{z}_0$:

Algorithm 1 Online RLS for Low-Rank RNNs

```
 1: Inputs: target trajectory $\{\mathbf{z}_t\}_{t=0}^{T}$, step size $dt$.
 2: Initialize: Basis parameters: $\mathbf{m}$, bias $\mathbf{b}$, weights $\mathbf{n} \leftarrow \mathbf{0}$, Precision $P \leftarrow \lambda^{-1}\mathbf{I}$
 3: for $t = 1$ to $T$ do
 4:     Basis vector $\phi_t \leftarrow \phi(\mathbf{m}\,\mathbf{z}_t + \mathbf{b})$
 5:     Target derivative $y_t \leftarrow \dfrac{\mathbf{z}_t - \mathbf{z}_{t-1}}{dt}$        (finite difference)
 6:     Prediction $\hat{y}_t \leftarrow \mathbf{n}^\top \phi_t - \mathbf{z}_t$
 7:     Error $e_t \leftarrow y_t - \hat{y}_t$
 8:     Gain $k_t \leftarrow \dfrac{P\,\phi_t}{1 + \phi_t^\top P\,\phi_t}$
 9:     Weight update $\mathbf{n} \leftarrow \mathbf{n} + k_t\,e_t$
10:     Covariance update $P \leftarrow P - k_t\,\phi_t^\top P$
11: end for
```

C General formulation & application to binary decision making task

We apply our framework to a specific group of binary decision making tasks commonly observed in systems neuroscience. In this task, a rat accumulates evidence of auditory pulses over time from clicks on its left and right side. At the end of the stimulus period, the rat must turn to the side which produced more clicks, and is rewarded for inferring this correctly. It has been shown that multiple underlying dynamical portraits could represent this behavior [39]. We thus show applicability of our method by using it to recover the autonomous and input driven dynamics on four separate synthetically generated dynamic portraits linked to this task [39]. Here, intuitively, the input dynamics encode for the accumulation of evidence based on the clicks, and a final decision to turn is made once the accumulation value reaches a specific attractor in the network. For instance, if the instrinsic dynamics encode a bi-stable attractor, each of the end points represent a specific decision, and the inputs move the dynamics along a line between them [38]. Additionally, consistent with previous studies, we model our simulations to provide equal weights to left and right clicks but with opposite magnitudes.

We model four flow fields representing intrinsic dynamics, namely a bi-stable attractor, a line attractor, a non-canonical line attractor and the flow field inferred from [39]. More formally, they are given as follows -

$$\begin{aligned}
&\text{Bistable attractors:}\\
&\qquad dz_1 = 10z_1(0.7+z_1)(0.7-z_1)dt + cudt\\
&\qquad dz_2 = -10z_2dt\\
&\text{Classic DDM - line attractor:}\\
&\qquad dz_1 = \begin{cases} cudt & z_1 \in (-0.7, 0.7)\\ 10z_1(0.7-z_1)(0.7+z_1)dt & z_1 \notin (-0.7, 0.7)\end{cases}\\
&\qquad dz_2 = -30z_2 \qquad\qquad (18)\\
&\text{Non-canonical line attractor:}\\
&\qquad dz_1 = 5z_2\\
&\qquad dz_2 = -5z_2dt + cudt\\
&\text{Unsupervised model:}\\
&\qquad dz_1 = 5z_1(0.85+z_1)(0.85-z_1)dt + cudt\\
&\qquad dz_2 = 5(0.5|z_1| + 0.1)(z_1 - 1.2z_2)
\end{aligned}$$

Here, z_1, z_2, represent the two latent dimensions, u represents the magnitude of the input clicks, and c represents if its positive or negative.
Critically, we observe the input dynamics lie in a dimension *parallel* to the recurrent activity. Or alternatively, drive the system in the dimensionality spanned by the recurrent activity. We thus present a general formulation of our equations to model these input dynamics. Following Eqn 5, for a scalar $\mathbf{z}$, we now not only observe orthogonal ($\mathbf{b} = \mathbf{b}_{perp}$) neuron specific inputs, but additional input dynamics that influence the recurrent activity ($\mathbf{b}_{par}$, spans the same direction as $\mathbf{m}$), thus updating Eqn 5 as :

$$\mathbf{x}(t) = \mathbf{m}\mathbf{z}(t) + \mathbf{b}_{par}\mathbf{v}_{par}(t) + \mathbf{b}_{perp}\mathbf{v}_{perp}(t), \qquad (19)$$

where $\{\mathbf{v}_{par}(t), \mathbf{v}_{perp}(t)\}$ represent the low-pass filtered inputs which drive activity along and perpendicular to the recurrent dimensions respectively.

Our goal of embedding the ODE $g(\mathbf{z})$ into the network can now be viewed as setting the model parameters so that

$$g(\mathbf{z}) + \mathbf{z} \;\approx\; \mathbf{n}^\top \phi(\mathbf{m}\mathbf{z} + \mathbf{b}_{par}\mathbf{v}_{par}(t) + \mathbf{b}_{perp}v_{perp}(t)) \qquad (20)$$

This allows us to follow a similar setup to our discussions in Sec. 3, with the exception that auditory inputs are applied along $\mathbf{b}_{par}$ or $\mathbf{b} = \mathbf{b}_{perp}$, or both.

As shown in Fig 10, each row represents one of the above dynamical regimes. The first column represents the dynamics along z_1, or z_2, and the RNN fitted version. Next, we model two right (or positive) clicks at $t = 0.5$ and $t = 1$ second and a single left (negative) click at $t = 2.5$ second. The second column represents the ODE when we start from ($z = 0$), pushed by these input dynamics, for our fitted RNN dynamics (Eqn 6) against the true ODE (computed using Euler method). Lastly, we also recover the underlying flow fields, as indicated by the last column. In Fig 11, we embed a non-canonical line-attractor in which input axis is perpendicular to the line attractor and non-normal dynamics give rise to movement along the line attractor. We successfully embedded all three of these systems with rank 1 RNNs. Lastly, we also embed a system with rotational dynamics between fixed points with integration along the diagonal between them. This is done through a rank 2 RNN with inputs along each of the directions spanned by $\mathbf{b}_{par}$(Fig. 11 B). This proves the flexibility of our framework in embedding dynamics associated with neuroscience tasks.

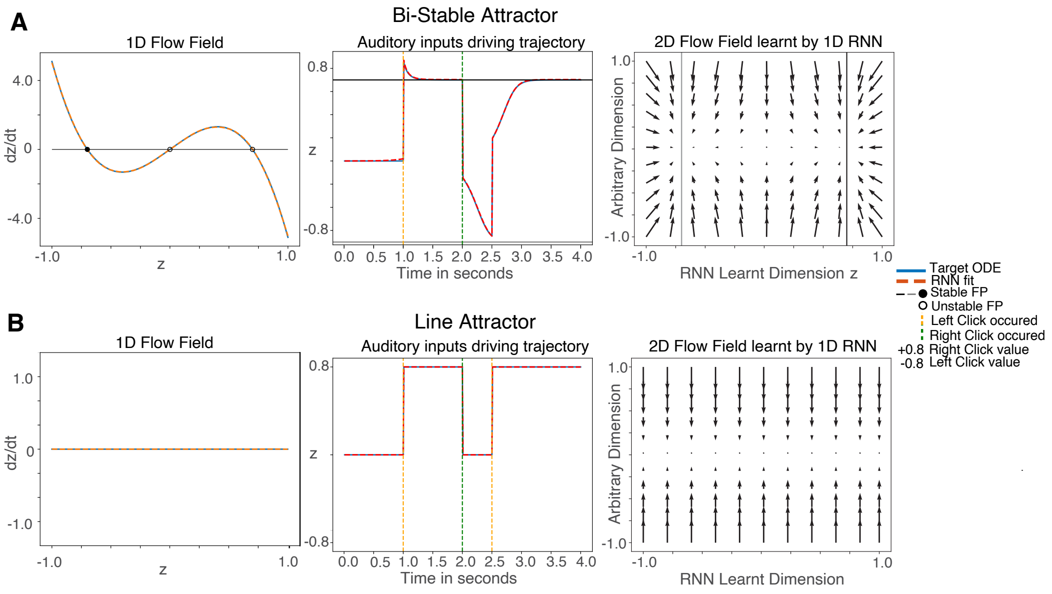

Figure 10: Two different dynamical portraits for binary decision making task: **(A)** bi-stable attractor ODE and **(B)** line attractor ODE. First column represents the true underlying ODE and the RNN estimate learned using least squares. Second column depicts a sample trajectory driven by momentary input clicks. A right click creates a drift towards the positive stable fixed point where as a left click, towards the negative stable fixed point for A. For B, accumulation along the line takes place with no diffusion. Third column represents the flow-field estimated by the RNN.

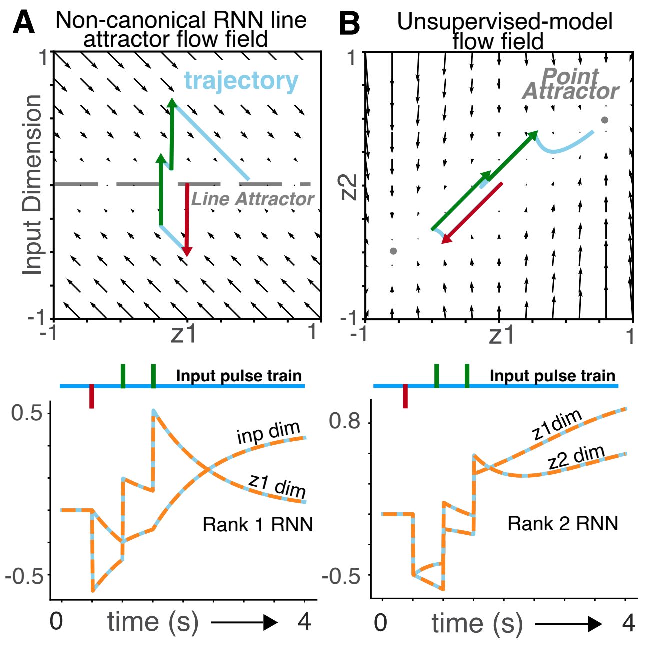

Figure 11: Two additional dynamical portraits for binary decision making task. Top: flow-field for each ODE, with input driven trajectory highlighted in blue. Bottom: true and fitted trajectories over time for each dimension.

D OMP algorithm and it's application to a limit cycle ODE

The detailed algorithm for OMP is given here:

Algorithm 2 OMP for finding smallest RNN

```
1: Select a grid of values $\mathbf{z}$.
2: Create global basis set $\Phi$ using uniformly sampled $\mathbf{m}, \mathbf{b}$ values.
3: Initialize $n$ weights using linear decay term only: $n_0 = -(\mathbf{z}^\top \mathbf{z})^{-1} \mathbf{z}^\top g(\mathbf{z})$.
4: Initialize residual: $r_0 = g(\mathbf{z}) - n_0 * (-\mathbf{z})$
5: Initialize solution basis set, $\Phi_0 = \emptyset$.
6: At each iteration $t$:
       1. Find basis vector with highest correlation with residual:
              $$i_t = \arg\max_i ||\Phi_i^T \mathbf{r}_{t-1}|||$$   (21)
       2. If entry $i$ is not in the solution basis:
              • Add new entry to the solution basis, $\Phi_t \leftarrow \Phi_i$
              • Solve to find new linear weights $[n_{0_t}\ \mathbf{n}_t']$ using Eqn 8
              • Solve to find new linear weights $\mathbf{n}_t'$ using Eqn 8
              • Compute the updated residual:
              $$r_t = g(\mathbf{z}) - \begin{bmatrix} n_{0_t}(-\mathbf{z}) \\ \mathbf{n}_t'^\top \Phi_t \end{bmatrix},$$   (22)
       3. Check for termination based on a predefined sparsity threshold
              $$d' = \mathrm{len}(\Phi_t)$$   (23)
```

D.1 Smallest RNN for 2D Limit Cycle

Following our discussion on the multi-dimensional case and the smallest RNN (Sec. 3.1, 5), we apply our framework to learn the smallest number of neurons needed to fit an RNN for the limit cycle flow-field (equations provided in SI. A.2). Specifically, we apply both our OMP and COMP method to greedily add neurons that best approximate the target ODE. Fig 12 highlights the advantage of our COMP and OMP methods in designing small RNNs. Additionally we note, for our COMP method, with just 20 neurons the ODE fits are qualitatively similar to the true target, with much lower MSE values compared to OMP. This showcases the advantage of COMP as the basis parameter space increase.

D.2 Parameter distribution of random basis for OMP

In this section we delve into the role of the distribution from which the random basis is sampled. As shown in Section 5, each basis function approximates the ODE ($g(\mathbf{z})$) over some finite domain ($\mathbf{z}$). Thus, first, it is critical the basis functions span the domain of the function being approximated. Second, these functions need not be odd symmetric and hence basis functions need to also be shifted to capture these movements. As shown in Fig 13), as long as these properties are met (i.e both the uniform grid and standard normal generate basis functions in the same domain, with the same offset ranges), the exact underlying distribution from which the basis functions are drawn does not play a critical role when finding the smallest low-rank RNN. This can be seen as the MSE values follow similar trends with greedy addition of basis functions (panel D). Qualitatively, this can also be observed via similar reconstruction of the ODE across iterations of OMP (panel A,B). Note however, by changing the distribution from which Φ is drawn the exact basis picked are different, as the global optimal basis are no longer the same (panel C).

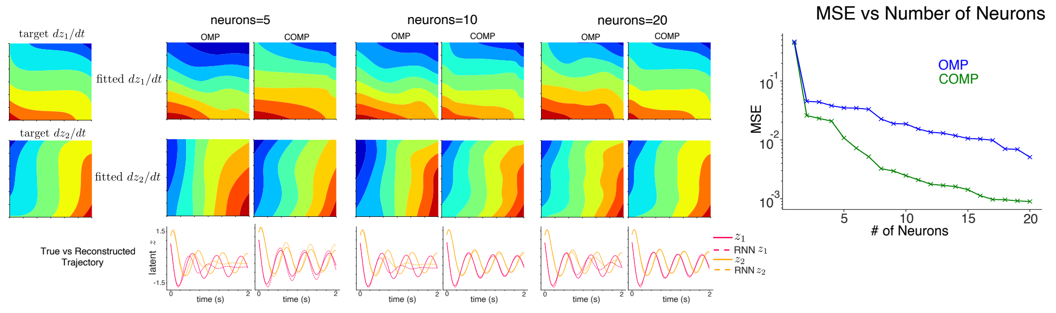

Figure 12: COMP and OMP for 2d Limit Cycle. The first row depicts the estimated flow-field for dimension one. The second row depicts the estimated flow-field for dimension two. Last row shows true vs the RNN reconstructed trajectory for both OMP and COMP. We show fits and reconstructions for 5, 10, 20 neurons that are added via OMP and COMP respectively. Right most panel depicts the mean squared error (on log-scale) as a function of the number of neurons. Note COMP shows much steeper drops in MSE, compared to OMP.

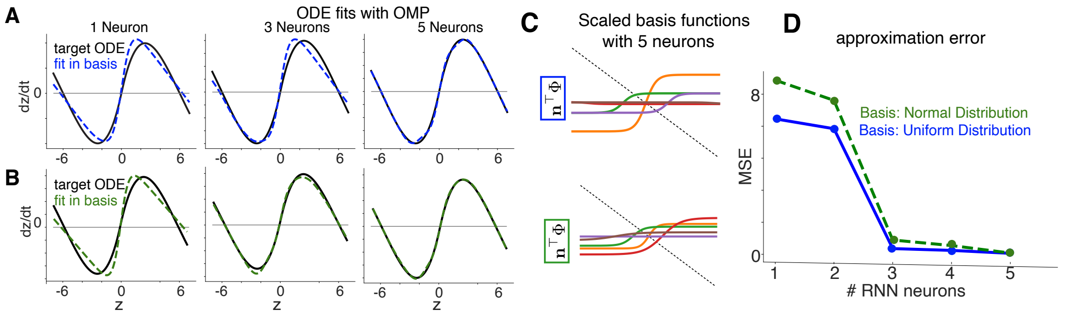

Figure 13: Influence of distribution of basis functions. **(A,B)** RNN estimated fit of Bi-stable attractor ODE the true underlying ODE over 1,3,5 iterations of OMP. In the top row basis functions (both m_i and $\mathbf{b}_i$) are generated over a uniform grid spanning $+1$ to -1. Alternatively the bottom row consists of basis functions generated from a standard normal (i.e $m_i \sim \mathcal{N}(0,1)$, and $\mathbf{b}_i \sim \mathcal{N}(0,1)$). **(C)** Scaled basis functions selected after 5 OMP iterations, with the top row drawn from the dniform distribution and the bottom row from the normal distribution. **(D)** Mean squared error (MSE) between target ODE and RNN approximation as a function of the number of RNN neurons added by OMP (blue: basis functions drawn from uniform grid, green: basis functions drawn from standard normal).

E Additional training details

E.1 Backprop comparison for a binary decision making ODE

In Section 4, both our framework and the networks trained with Backprop are trained and tested from a set of teacher trajectories, which are simulated from the underlying ODE (eg., in the binary decision-making task, trajectories originate from random initial conditions and evolve toward one of two fixed points). To generate each trajectory, we used Euler integration with a time step of $dt = 0.01$ over a duration of 4 seconds, yielding 400 time steps per trajectory. A total of 160 unique initial conditions were uniformly sampled along the z-axis. Of these, 150 were used for training and the remaining 10 for testing. Each of the networks trained via BP in Fig 3 were trained for 15 epochs, with a batch size of 10 per epoch. Thus, a total of 150 gradient steps were performed (performance plateaued at 100 gradient steps). Additionally, each of the networks were trained over three random seeds of initializations, where parameters were initialized from standard normal distributions. The values reported in Fig 3 correspond to the best performing seed. Lastly, to compare performance we trained our networks via our online RLS implementation. Once training was complete (using the 150 training trajectories), we used the final $\mathbf{n}$ weight to test performance.

We report training times in Table 1. Note, our framework provides significantly faster training.

Table 1: Training Time For Binary-Decision Making Task

Model Type	Size	Time(s)
Low Rank ($r = 1$)	5	62.419
Low Rank ($r = 1$)	10	62.468
Full Rank	2	29.161
Full Rank	3	29.209
Full Rank	5	29.025
Full Rank	10	29.392
Full Rank	50	28.998
Our Model	5	0.069

E.2 Target tracking task: Compare networks with optimal bases vs standard normal bases

To compare performance for networks trained with optimized basis against those trained with the standard normal basis, we derive a target matching problem from the ODE presented in Figure 5 (Panels A and B). Specifically, we used a set of four starting locations in $\mathbf{z}$ given by: $[7.92, 4.72, 2.3, -7.36]$. We then rolled out the dynamics (as per the ODE) using an Euler integration for a total of a 1000 time-steps, with $dt = 0.1$. Each of these trajectories (originating from each of the start locations) converged to a specific stable fixed point. We then compared rank 1 RNNs trained via our Online Method (RLS) and those trained with BPTT. Our RLS method achieves near perfect performance after a single epoch, while BPTT trained networks were trained for 5 epochs. MSE results presented are averaged over 5 random seeds of initialization.

E.3 FORCE Comparisons

E.3.1 Lorenz Attractor Trajectory

Following our discussion in Sec. 4, we present an additional evaluation using a more challenging target trajectory: the Lorenz attractor, a well-known chaotic system defined by the set of coupled nonlinear differential equations

$$\frac{dx}{dt} = \sigma(y - x), \quad \frac{dy}{dt} = x(\rho - z) - y, \quad \frac{dz}{dt} = xy - \beta z, \tag{24}$$

using standard parameters $\sigma = 10$, $\rho = 28$, and $\beta = 8/3$. We simulated the trajectory using Euler integration with a time step of $dt = 0.01$ for a total of $T = 3000$ steps (30 seconds of data), and used the scaled $x(t)$ signal as the target output (as in [9]). While our method was trained on (and able to reconstruct) all three variables $Z = [x(t), y(t), \text{ and } z(t)]$, only reconstructions of $x(t)$ are shown for comparison, as this is the only signal used in the FORCE training objective [9]. Specifically in our case, this can be formalized as a rank-3 RNN, written as the problem of fitting three different nonlinear functions $\frac{dx}{dt}$, $\frac{dy}{dt}$ and $\frac{dz}{dt}$ using three different linear combinations of the same 3D basis functions:

$$\begin{bmatrix} \frac{dx}{dt} \\ \frac{dy}{dt} \\ \frac{dz}{dt} \end{bmatrix} \approx -\begin{bmatrix} x \\ y \\ z \end{bmatrix} + \begin{bmatrix} \mathbf{n}_1^\top \phi(MZ + \mathbf{b}) \\ \mathbf{n}_2^\top \phi(MZ + \mathbf{b}) \\ \mathbf{n}_3^\top \phi(MZ + \mathbf{b}) \end{bmatrix}, \tag{25}$$

where $M = [\mathbf{m}_1 \mathbf{m}_2 \mathbf{m}_2]$ is a $d \times 3$ matrix, $\mathbf{b}$ is once again a column vector of offsets, and we have assumed a constant filtered input, $\mathbf{v} = 1$.

We compare networks trained using our online learning framework against those trained with the FORCE algorithm. For FORCE, we used a recurrent gain of $g = 1.5$ and trained each network across 10 random seeds; our method was similarly evaluated with the same number of seeds. Fig 14 reports mean squared error (MSE) averaged across seeds, along with representative trajectory reconstructions.

As in previous experiments, our method consistently achieves lower MSE with fewer neurons. Qualitatively, this is also evident in the trajectory reconstructions: our networks produce more accurate fits at smaller sizes ($N = 16, 64$) than FORCE, which fails to reliably capture the signal until larger networks (for instance showed with $N = 1024$). Additionally, this further highlights that our networks converge more rapidly than those trained with FORCE.

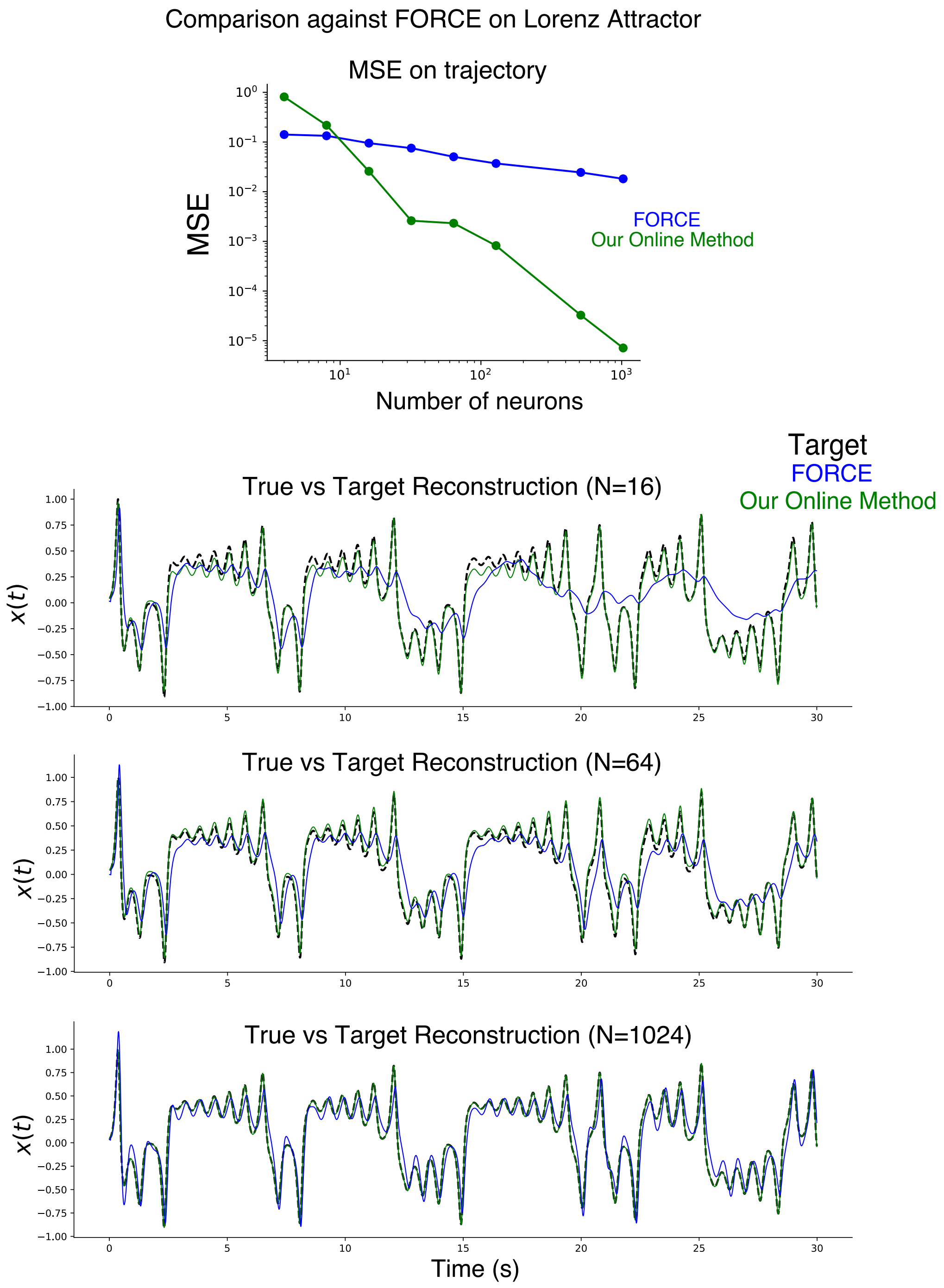

Figure 14: **Top Row:** Mean squared error (MSE) in log scale across networks of varying size (left). **Bottom Rows:** True vs reconstructed $x(t)$ trajectory from the Lorenz system, (green our method, blue FORCE) for networks of size $16, 64, 1024$.

E.3.2 Application to noisy data

We further validate our framework by discussing it's application to noisy data. Specifically, we simulated a target signal for a total of $T = 1000$ seconds. This signal was sampled with a discrete time bin of $dt = 0.1$, thus 10,000 time steps of the target wave were obtained. We then added independent gaussian noise: $\mathcal{N} \sim (0, 0.05)$, at each time step of the trajectory to obtain the noisy target (also used in FORCE [9]). While the target output is a 1-d signal, we used the trajectory and it's two cumulative sums to fit our networks (thus needing rank 3 network). We trained RNNs using our RLS method, FORCE and BPTT (rank $3, 4$). To ensure a consistent comparison, in Fig. 15 we report the training MSE (averaged across 5 seeds) after one epoch: a single pass over the $10,000$-step sequence, across all methods. We see highest performance with our RLS method. Additionally, both RLS and FORCE achieve near-perfect performance in a single pass, while BPTT typically requires 5–8 epochs to reach comparable errors.

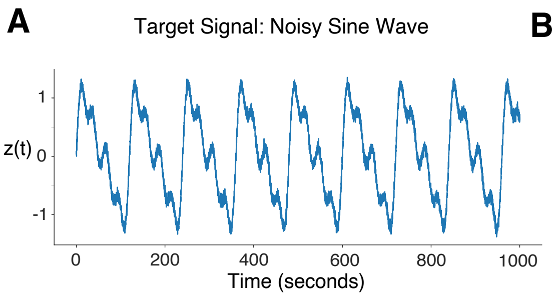

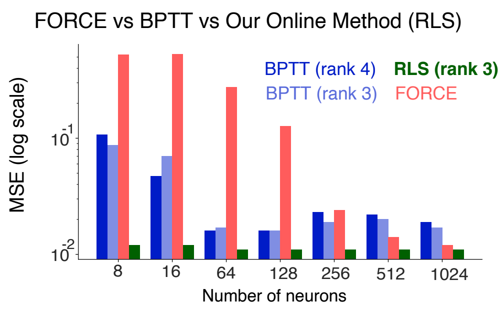

Figure 15: Networks fit on a noisy sum of four sinusoids target signal. **A**: Target trajectory sampled for $T = 1000$ seconds. **B**: Training Mean Squared Error (in log scale) of networks trained with FORCE, BPTT and our Online Method (RLS)

E.3.3 Additional discussion on our online (RLS) method and the FORCE Framework

Below we discuss some ways in which our methodology differs from the FORCE/FULL-FORCE [9, 10] training schemes.

1. **Initialization with Full-Rank weight matrix:** FORCE/FULL-FORCE methods require full rank-initializations, and learn low-rank updates on this initilalization over time. This comes at the cost of interpretibility as the dynamics of such networks need to be analysed post training through methods such as PCA. On the other hand, our *offline and online* framework directly models the latent low-dimensional dynamic and doesn't ever need full-rank initializations.
2. **Senstive to initialization and requires multiple epochs:** One of the motivations of FORCE is that it introduces the benefits of training networks that exhibit chaotic activity prior to training. While powerful, it is observed this results in these networks needing multiple epochs/iterations. Additionally, these networks exhibit stochastic results based on initialization (e.g based on the parameter g). In contrast, our methods provide a deterministic closed form updates.
3. **Doesn't directly embed an ODE, but produces a set of target trajectories:** A stark difference between our *offline* framework is unlike other training methodologies similar to FORCE and FULL-FORCE that can only be trained against target trajectories, we can also directly model the underlying ODE. Thus, in cases where such a hypothesized ODE exists, we can represent the entire space of the low-dimensional dynamic.

F Embedding higher dimensional ODEs

To highlight the ability of our framework to embed higher dimensional ODEs, we train a network to perform the n-bit flip flop task [12]. Specifically, we consider the case where $n = 10$. In this case, the network receives 10 binary inputs at random times, and produces 10 binary outputs. The network is expected to maintain it's output if the inputs received are the same, or alternatively switch it's output if the opposite input pulse is presented. We successfully embed such a task using a rank 10 network with 10 neurons. We design our networks such that each neuron is required to keep track of a single input pulse, thus requiring 10 neurons. Note, this could be arbitrarily scaled up to any number of input pulses, by simply scaling up the number of neurons in the network. In Fig. 16, each neuron is presented with random positive or negative input pulses in blue, to which it must respond appropriately. Our method generates the required output as seen via the activity $(x(t))$ of 4 example neurons from this network. The network was simulated for $T = 50$ seconds, sampled at $dt = 0.01$. Concretely, this was achieved by rolling out the equivalent high-dimensional network dynamics given by:

$$\dot{\mathbf{x}} = -\mathbf{x} + MN^\top \phi(\mathbf{x}) + B\mathbf{u} \tag{26}$$

In our case, M, N, B are randomly drawn from standard normal distributions. $\mathbf{u}$ represents the input pulse train seen in blue, and the vector of neural activity $x(t)$ represents the desired output.

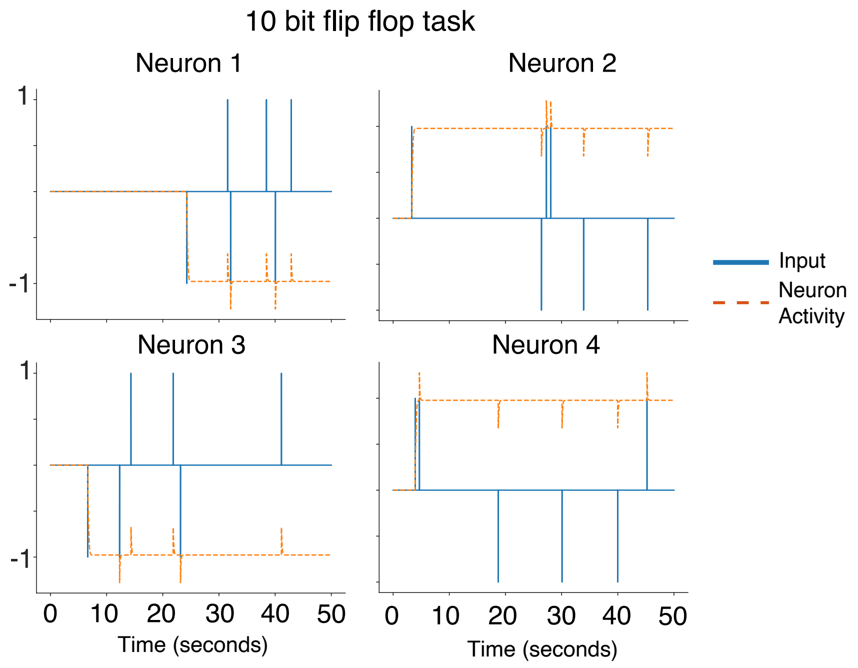

Figure 16: RNN generating appropriate response for the 10 bit flip-flop task. Neuron Activity, $x(t)$ of 4 example neurons is shown.